


FULL PAPER

Open Access



Evaluation of a method to retrieve temperature and wind velocity profiles of the Venusian nightside mesosphere from mid-infrared CO₂ absorption line observed by heterodyne spectroscopy

Kosuke Takami¹, Hiromu Nakagawa¹, Hideo Sagawa², Pia Krause³, Isao Murata⁴, Yasumasa Kasaba^{5*} , Takeshi Kuroda¹, Shohei Aoki^{6,7}, Toru Kouyama⁸, Theodor Kostiuik⁹, Timothy A. Livengood⁹ and Gabriella Gilli¹⁰

Abstract

We evaluated a method for retrieving vertical temperature and Doppler wind velocity profiles of the Venusian nightside mesosphere from the CO₂ absorption line resolved by mid-infrared heterodyne spectroscopy. The achievable sensitive altitude and retrieval accuracy were derived with multiple model spectra generated from various temperature and wind velocity profiles with several noise levels. The temperature profiles were retrieved at altitudes of 70–100 km with a vertical resolution of 5 km and a retrieval accuracy of ± 15 K. The wind velocity was also retrieved at an altitude of approximately 85 km with a vertical resolution of 10 km and a retrieval accuracy of ± 25 –50 m/s. In addition, we studied an event and applied our method to spectra obtained by the HIPWAC instrument attached to the NASA/IRTF 3-m telescope on May 19–22, 2012. Retrieved wind velocities in a latitude of 33° S at 3:00 LT were interpreted as subsolar-to-antisolar (SS-AS) flows at altitudes of 84 ± 6 km and 94 ± 7 km, and they were stronger than expected. This result suggested that the transition between the retrograde superrotational zonal (RSZ) wind and SS-AS flow may occur at altitudes below 90 km which previously was predicted to be the transition region. This work provides a basis for our analysis of further observations obtained by a mid-infrared heterodyne spectrometer MILAHI attached to the Tohoku University 60-cm telescope at Haleakalā, Hawaii.

Keywords: Venus, Mesosphere, Temperature, Wind velocity, Mid-infrared heterodyne spectroscopy, CO₂ absorption line

Introduction

The global wind pattern in Venusian mesosphere has often been discussed with two components, that is the subsolar-to-antisolar (SS-AS) flow in upper part and the retrograde superrotational zonal (RSZ) wind in lower part (Bougher et al. 2006; Gérard et al. 2017).

The SS-AS flow is considered to dominate the global circulation pattern in the lower thermosphere at the altitudes above 120 km where the day and night temperature difference becomes significant (> several 10s K) and the wind is driven by such a temperature gradient. Several observations support the presence of SS-AS flows at the altitudes of ~ 95 –120 km (Gérard et al. 2017). The SS-AS flow at $\sim 97.4 \pm 2.5$ km was inferred from night-glow tracking of O₂ observed by the Visible and Infrared Thermal Imaging Spectrometer (VIRTIS) aboard VEX (Drossart et al. 2007; Gorinov et al. 2018). The Doppler

*Correspondence: kasaba@pparc.gp.tohoku.ac.jp

⁵ Planetary Plasma and Atmospheric Research Center, Graduate School of Science, Tohoku University, Sendai, Miyagi 980-8578, Japan
Full list of author information is available at the end of the article

wind velocities at the altitudes at ~ 95 – 115 km were also derived from the CO LTE (local thermodynamic equilibrium) absorption lines observed in the sub-millimeter range (e.g., Lellouch et al. 2008; Moullet et al. 2012; Clancy et al. 2012b, 2015). These sub-millimeter observations showed that the amplitudes of SS-AS and RSZ components are highly variable both in time and space. For example, the non-presence of SS-AS flow was observed in some case for reasons that are still not understood.

For this altitude range, the numerical simulations showed that atmospheric circulation distinctly changes due to the momentum transport from lower atmosphere by an upward propagating gravity wave (GW) (Hoshino et al. 2013; Nakagawa et al. 2013). An improved version of a ground-to-thermosphere Venus general circulation model (GCM) including a non-orographic GW parameterization developed at Institut Pierre Simon Laplace/Laboratoire de Météorologie Dynamique (IPSL/LMD) (Gilli et al. 2017) provides a better representation of temperature profiles at altitudes above 100 km, such as those observed by the SPICAV (Spectroscopy for the Investigation of the Characteristics of the Atmosphere of Venus) and SOIR (Solar Occultation at Infrared) instruments on Venus Express.

At lower altitudes, the RSZ wind in the direction of the Venusian rotation maximizes to greater than 100 m/s at approximately the cloud top altitude (~ 70 km), as has been derived from cloud tracking observed by the Venus Monitoring Camera (VMC) aboard Venus Express (VEX) (e.g., Khatuntsev et al. 2013, 2017; Kouyama et al. 2013) and Akatsuki UV Imager (e.g., Horinouchi et al. 2018).

The vertical transition between the SS-AS flow and the RSZ wind was estimated with a thermal wind equation by Seiff et al. (1980) from the pressure gradient in the downside between the Pioneer Venus North probe (59.3° N, LT 3:35) and the Day probe (31.2° S, LT 6:46) to reach altitudes of 100 km. This result showed the presence of RSZ wind with the velocity of greater than 120 m/s at the altitudes of 70–90 km. However, thermal wind derived from the temperature field retrieved from VEX VIRTIS-M data showed a smaller velocity that can reach 0 m/s at the altitude of 80 km at midnight, 23–01 LT (Peralta et al. 2017). Ando et al. (2018) also showed an abrupt decrease of the zonally averaged zonal wind to 44–64 m/s at the altitudes of 75–85 km derived from the dispersion relationship of the internal GWs observed as a vertical wave structure with the Akatsuki radio occultation measurements. However, direct wind observations have not been conducted at altitudes of 70–90 km.

As another observation tool, the Doppler wind velocity was directly derived from the CO₂ non-LTE emission lines observed on the dayside by mid-infrared heterodyne spectroscopy (Sornig et al. 2008, 2012, 2013). This

method can probe the wind velocity at 110 ± 10 km (López-Valverde et al. 2011). Goldstein et al. (1991) performed the first measurement at this altitude range with heterodyne spectroscopy and obtained a global circulation including SS-AS flow. The dayside non-LTE CO₂ emission lines have been used for the retrieval of wind velocity and temperature profiles in the lower thermosphere at the altitude of 110 ± 10 km (e.g., Krause et al. 2018; Nakagawa et al. 2013; Sonnabend et al. 2008, 2010, 2012; Sornig et al. 2008, 2012, 2013).

CO₂ LTE absorption lines can be directly detected at altitudes of 60–90 km on the nightside by mid-infrared heterodyne spectroscopy. Stangier et al. (2015) retrieved temperature profiles with the instrument named Heterodyne Instrument for Planetary Wind and Composition (HIPWAC; Kostiuik et al. 2005) attached to the Cassegrain focus of the National Aeronautics and Space Administration (NASA) Infrared Telescope Facility (IRTF) 3-m telescope. Nakagawa et al. (2016) also demonstrated the possibility of the wind velocity retrieval with an accuracy of 15–25 m/s for altitudes of 85–95 km.

This work follows Stangier et al. (2015) and Nakagawa et al. (2016), and presents a new attempt to retrieve Doppler wind velocity as well as temperature profile in the Venusian nightside from the CO₂ absorption line resolved by mid-infrared heterodyne spectroscopy. The target sensitivity of the Doppler wind velocity retrieval aims to constrain the vertical transition of RSZ wind at altitudes below 100 km.

The structure of this paper is as follows. First, we describe the retrieval method and validate it in terms of the dependence of the retrieval results on the a priori profile. Next, the sensitive altitude and retrieval accuracy are evaluated using multiple model spectra generated from various temperature and wind velocity profiles with several noise levels. Finally, we apply the method to the Venusian nightside spectra observed by a mid-infrared heterodyne spectrometer HIPWAC attached to IRTF on May 19–22, 2012. The data were reselected and reprocessed from the dataset analyzed by Stangier et al. (2015). We validate our scheme by comparing with both retrieved temperature profiles.

In this work, we aimed to achieve the wind velocity and temperature retrieval requirements with an accuracy better than ± 50 m/s and ± 15 K. For the wind velocity retrieval, a numerical model study showed that the transition between SS-AS flow and RSZ wind occurred at an altitude of ~ 90 km (Alexander 1992). The wind profile in the downside was gradually varied from ~ 50 m/s eastward at 80 km to ~ 50 m/s with westward direction at 100 km. For observational identification of this transition, the accuracy of the wind velocity retrieval should be better than ± 50 m/s. For the temperature retrieval, we

used as reference a VEX SPICAV result which showed the warm layer. This is 30–70 K higher than temperature obtained by previous measurements, and it was interpreted to be caused by the adiabatic heating during the air subsidence of the SS-AS flow above 120 km (Bertaux et al. 2007; Gérard et al. 2017). For observational identification of such warming, the retrieved temperature accuracy should be better than ± 15 K.

Sequence of retrieval and dependence on a priori profiles

In this study, we used a model named AMATERASU (Advanced Model for Atmospheric Terahertz Radiation Analysis and Simulation; Baron et al. 2008) for temperature and wind velocity retrievals from the CO₂ LTE absorption lines. This model consists of a forward model which synthesizes observation spectra and an inversion model which performs retrieval of physical parameters from observations using a priori values as regularization constraints. It was originally developed for the retrieval of terrestrial atmosphere remote sensing in sub-millimeter wavelength (e.g., Baron et al. 2011), and modified for the application of the Venusian atmosphere. We set a reference Venusian atmosphere model based on the temperature and pressure profile from the Venus International Reference Atmosphere, VIRA (Seiff et al. 1985). The values above 100 km are taken from Seiff and Kirk (1982). In our work, both are connected with spline interpolation in the 95–105 km range (hereafter referred to as “VIRAex”). CO₂ line opacity is calculated with spectroscopic database of HITRAN 2012 (Rothman et al. 2013). The absorption coefficient of the cloud was calculated from the particle densities of each cloud mode summarized in Table 2 of Eymet et al. (2009).

Retrieval grid and retrieval sequence

In the forward model of our study, we set the temperature and wind velocity profiles at the altitude range of 0–140 km with 1-km steps (hereafter referred to as “full grid”). In the retrieval process, we use a coarser grid at same altitude range of 0–140 km (hereafter referred to as the “retrieval grid”). For temperature retrieval, we set up 29 layers with 5-km steps which were close to the scale height in the mesosphere. For wind velocity retrieval, the number of layers was reduced to improve the sensitivity of the retrieval, and 15 layers were set up with 10-km steps. The retrieval process was performed in a sequential manner as follows: (1) temperature retrieval was conducted with the retrieval grid (5 km step), with wind velocity fixed to 0 m/s at all altitudes. The retrieved temperature profile was used as an a priori temperature in the next step. (2) Wind velocity retrieval was conducted with the grid size of 10 km, and temperature was

also retrieved simultaneously. This is because the best fit spectrum could be achieved not only taking into account the frequency shift due to the wind velocity, but also by considering the radiance change by the temperature.

For the inversion process, the temperature and wind velocity profiles in the forward model with the full grid (1-km steps) were converted to those in the coarser retrieval grid (5-km steps in the temperature case and 10-km steps in the wind case). After the inversion process, the retrieved profile in the retrieval grid was linearly interpolated into the full grid for the next forward calculation to output the synthetic spectrum for the subsequent iteration. For obtaining the coarser retrieval grid, we need to define the grid points of altitudes with a certain step. By prior study, we knew that the different definition of the grid points of altitudes can lead the different wind/temperature in some cases. Therefore, we carefully attempt the grid points of altitudes as a free parameter for retrieval process, in addition to a priori profiles and continuum level. The retrievals are performed with 5 cases for temperature retrieval and 10 cases for wind velocity retrieval by shifting with 1-km step. At last, the profile of the best fit to observed spectrum is determined as the retrieved profile.

Dependence on a priori profiles

In this work, we create a priori temperature profiles based on VIRAex in the altitude of 0–140 km. The retrieved results can be affected by the condition of the a priori profiles. Although our inversion model uses a priori profiles based on VIRAex for regularization of the inverse problem, it is known that the temperature profile in Venusian mesosphere is highly variable, having temporal and spatial variations on the order of 20–30 K (e.g., Clancy et al. 2012a). Wind velocity profiles also show the large vertical gradient changing from the RSZ wind to the SS-AS flow on the order of 200 m/s. The full characteristics of those variabilities are not obtained yet, and the numbers of observational constraints are still limited. These facts make it difficult for us to prepare appropriate a priori profiles for each observation.

We treated the dependences on a priori profiles ε_{AD} as a part of total retrieval errors ε_{ret} , given by

$$\varepsilon_{ret} = \sqrt{\varepsilon_{noise}^2 + \varepsilon_{null}^2 + \varepsilon_{AD}^2}, \quad (1)$$

where ε_{noise} is the error from the noise in the observed spectrum, and ε_{null} the error from the components in the null space of the weighting function matrix used in the retrieval. In this subsection, ε_{ret} was studied, evaluated, and investigated using a priori profiles with various temperature and wind velocity profiles.

For the investigation of the dependence on a priori profiles, we first synthesized 5 model spectra as the emulations of the observed $^{12}\text{C}^{16}\text{O}_2$ P(12) absorption line profile at 951.19226 cm^{-1} (28,516,026.588 MHz) that was used in the event study described in “Retrieval from the CO₂ absorption spectra observed by HIPWAC in May 2012” section. Each of these 5 spectra was synthesized using different temperature profiles with specific temperature offsets at all altitudes from VIRAex, i.e., -30 K (cold case), -15 K (semi-cold case), 0 K (VIRAex case), $+15\text{ K}$ (semi-warm case), and $+30\text{ K}$ (warm case). Those offset values covered the observed temperature variation of $20\text{--}30\text{ K}$ (e.g., Clancy et al. 2012a). In these model spectra, the wind velocity profiles were commonly assumed as 0 m/s at all altitudes. Figure 1 shows the simulated 5 model spectra. White noise with root mean square (RMS) amplitude of $1.0\text{ erg/s/cm}^2/\text{sr/cm}^{-1}$ is included as the emulation of the real observed spectrum (corresponds to an integration time of a few hours).

Next, we retrieved the temperature and wind velocity profiles from the synthesized spectra with various a priori profiles. For the evaluation of the dependence on the a priori temperature profile, we prepared various a priori temperature profiles, $T'(z)$, as

$$T'(z) = \begin{cases} T(z) + \Delta T_{0-60} & (0 < z < 60) \\ T(z) + \frac{\Delta T_{110-140}}{110-60}(z-60) + \Delta T_{0-60} & (60 \leq z \leq 110) \\ T(z) + \Delta T_{110-140} & (110 < z < 140) \end{cases} \quad (2)$$

where z is the altitude in km, and $T(z)$ the VIRAex temperature profile. ΔT_{0-60} and $\Delta T_{110-140}$ are the offset temperature values. For this test, we used a constant ΔT_{0-60} below 60 km and $\Delta T_{110-140}$ above 110 km , and linearly interpolated between 60 and 110 km . ΔT_{0-60} and $\Delta T_{110-140}$ were independently set between -30 K and $+30\text{ K}$ with 5 K steps. Hence, there were 13 cases for ΔT_{0-60} and $\Delta T_{110-140}$ each, and a total of 169 a priori temperature profiles were prepared. For all profiles, the wind velocity profiles were set to 0 m/s at all altitudes. Some examples of model spectra calculated with these a priori profiles are shown in Fig. 1a (black lines).

For the evaluation of the dependence on the a priori wind velocity profile, we also prepared 41 a priori Doppler wind velocity profiles varied from -200 m/s to $+200\text{ m/s}$ with 10-m/s steps at all altitudes. (We set negative values for the line-of-sight wind moving away from observer, and positive for moving toward observer). This range covered the annual variation of the RSZ wind velocity within 120 m/s at the cloud top (Khatuntsev et al. 2014) and the enhanced SS-AS flow of $189 \pm 11\text{ m/s}$ at the altitude of $110 \pm 10\text{ km}$ (Sornig et al. 2013). For all cases, temperature profiles were set as VIRAex. Note that a Doppler shift of $\pm 100\text{ m/s}$

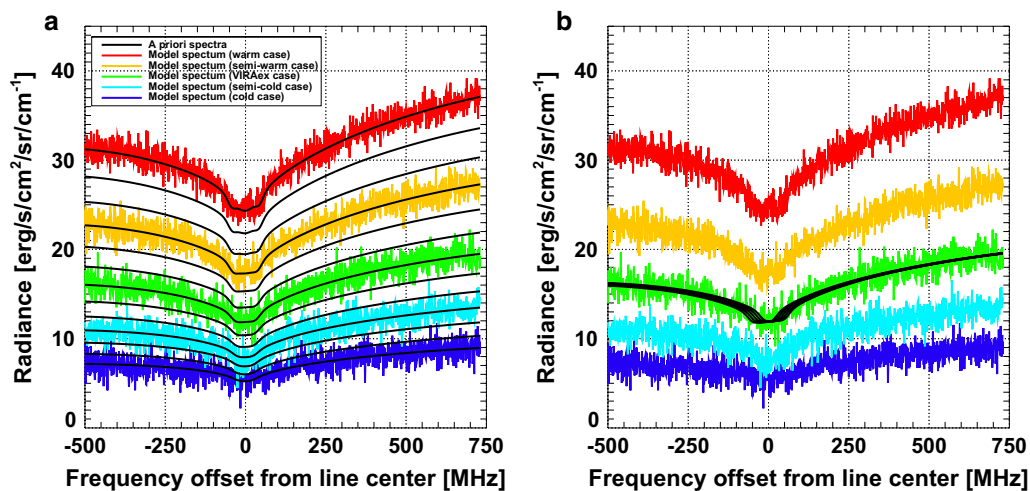


Fig. 1 Five model spectra as emulated CO₂ absorption line profile. Color lines show the synthesized spectra from the temperature profiles of -30 K (cold case, blue), -15 K (semi-cold case, sky blue), 0 K (VIRAex case, in green), $+15\text{ K}$ (semi-warm case, yellow), and $+30\text{ K}$ (warm case, red) cases from VIRAex. For all of these, the wind velocity profiles are set to 0 m/s at all altitudes. White noise with the RMS of $1.0\text{ erg/s/cm}^2/\text{sr/cm}^{-1}$ is added. **a** Black lines show examples of 13 a priori spectra generated from temperature profiles of $-30\text{--}+30\text{ K}$ from VIRAex with 5 K steps at all altitudes. The wind velocity profiles are 0 m/s at all altitudes. **b** Black lines show examples of 5 a priori spectra generated from the wind velocity profiles of $-200\text{--}+200\text{ m/s}$ at 100-m/s steps at all altitudes. The temperature profiles are VIRAex

approximately corresponds to the frequency shift of ± 10 MHz. Some examples of model spectra calculated with these a priori profiles are shown in Fig. 1a (black lines).

Figure 2 shows the temperature profiles retrieved from the model spectrum of the “VIRAex case”, as an example of the retrievals using different conditions for a priori temperature profiles. Figure 3 shows the wind velocity profiles retrieved from the model spectrum of the “VIRAex case” using 41 different a priori wind velocity profiles, as an example of the retrievals using different conditions for a priori wind velocity profiles. We have to note that blue cases and red cases led the different retrieved wind velocity values by ~ 20 m/s at ~ 85 km altitude. As we mentioned in the previous section, this is because of the difference of the defined retrieval grid for each retrieval. In this case, we got the two solutions of the convergence using all a priori wind velocity profiles.

Figure 4 summarizes 5 standard deviations of retrieved temperature profiles (Fig. 4a) and wind velocity profiles (Fig. 4b) retrieved from 5 model spectra shown in Fig. 1 with 169 a priori temperature profiles, and with 41 a priori wind velocity profiles. We interpreted these standard deviations as the error due to a priori profiles, ϵ_{AD} . In the temperature retrieval shown in Fig. 4a, ϵ_{AD} was lower than 10 K in the 70–100 km altitude range for the

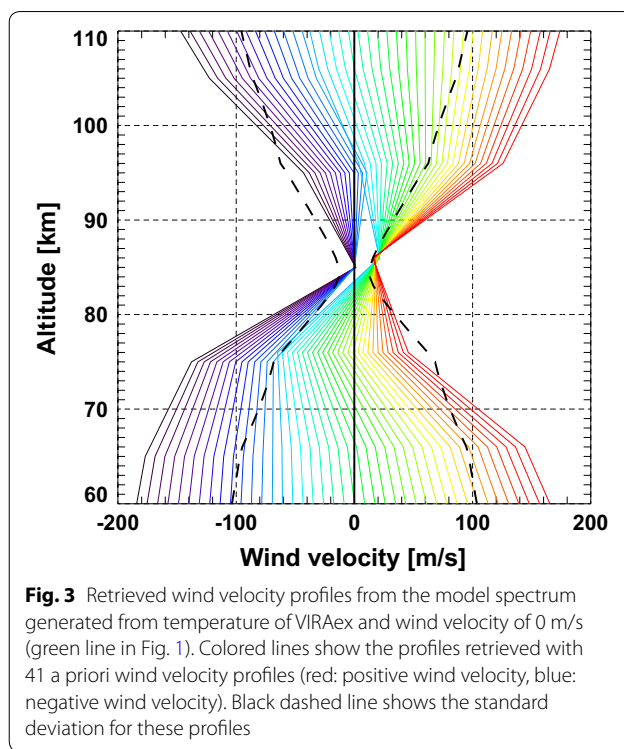


Fig. 3 Retrieved wind velocity profiles from the model spectrum generated from temperature of VIRAex and wind velocity of 0 m/s (green line in Fig. 1). Colored lines show the profiles retrieved with 41 a priori wind velocity profiles (red: positive wind velocity, blue: negative wind velocity). Black dashed line shows the standard deviation for these profiles

VIRAex, semi-warm, and warm cases. In the cold and semi-cold cases, ϵ_{AD} less than 10 K were only observed in

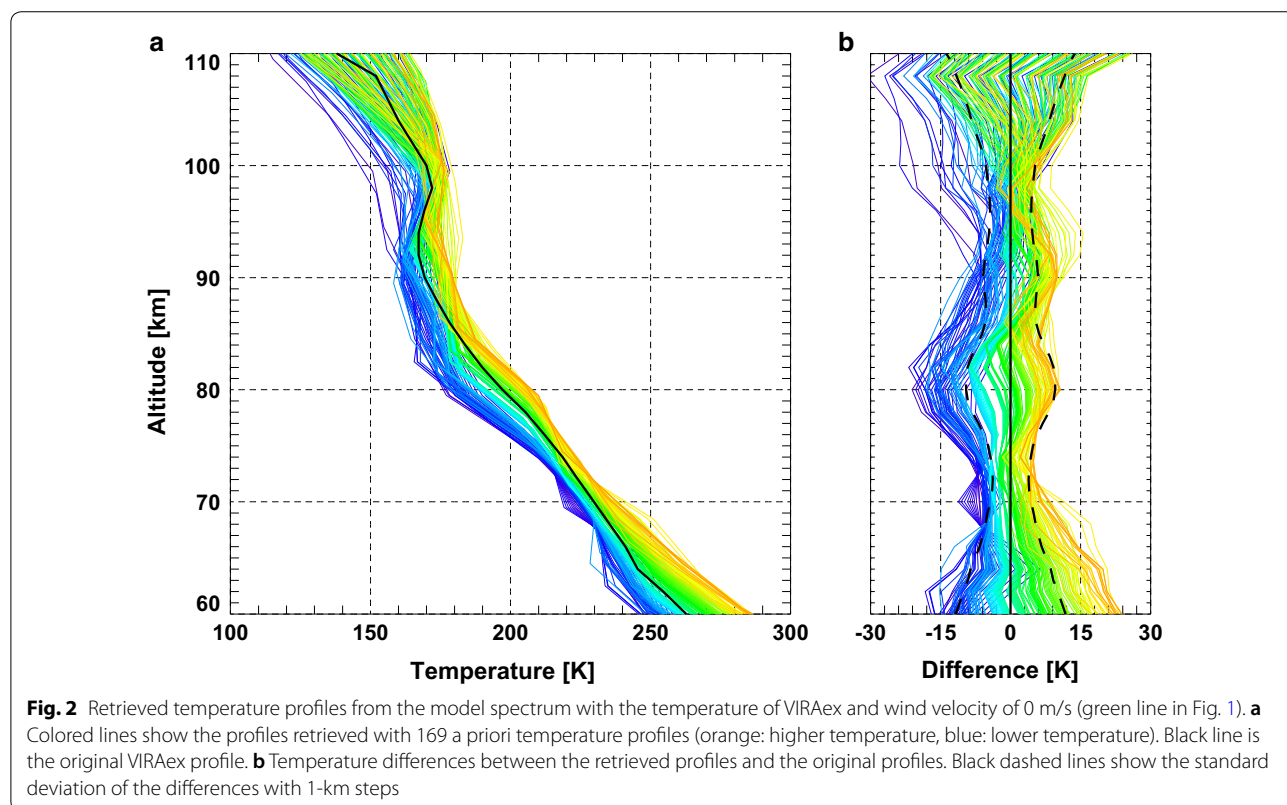
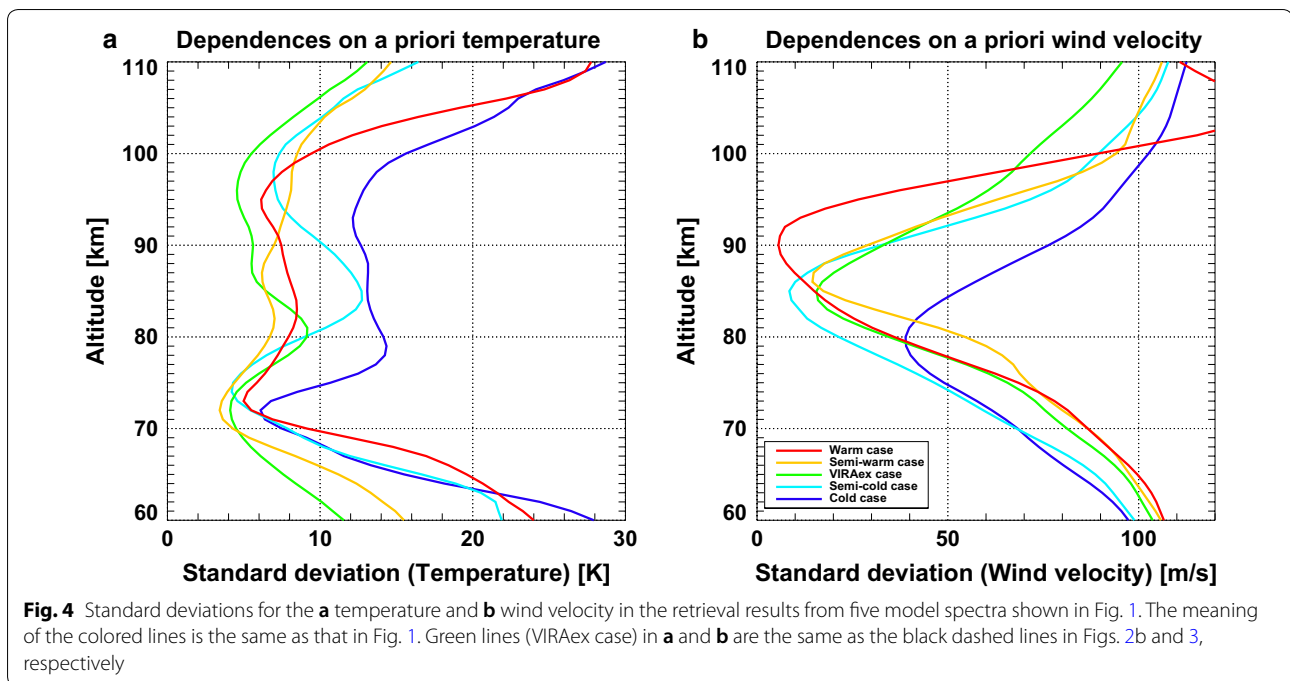


Fig. 2 Retrieved temperature profiles from the model spectrum with the temperature of VIRAex and wind velocity of 0 m/s (green line in Fig. 1). **a** Colored lines show the profiles retrieved with 169 a priori temperature profiles (orange: higher temperature, blue: lower temperature). Black line is the original VIRAex profile. **b** Temperature differences between the retrieved profiles and the original profiles. Black dashed lines show the standard deviation of the differences with 1-km steps



the 68–75 km and 68–81 km altitude ranges, respectively. (For $\varepsilon_{AD} \sim 10$ K, $\sqrt{\varepsilon_{noise}^2 + \varepsilon_{null}^2}$ must be within ± 11 K to achieve the total retrieval errors ε_{ret} within ± 15 K. This is related to the baseline requirement for the integration time in real observations.) In contrast, in the wind velocity retrieval shown in Fig. 4b, ε_{AD} of less than 25 m/s can be achieved at around 85 km in the semi-cold, VIRAex, semi-warm, and warm cases. In the cold case, the minimum error was ~ 40 m/s at the altitude of 80 km. (For ε_{AD} of 25–40 m/s, $\sqrt{\varepsilon_{noise}^2 + \varepsilon_{null}^2}$ must be within ± 43 –30 m/s to achieve the total retrieval errors ε_{ret} within ± 50 m/s. This is also related to the baseline requirement for the integration time in real observations.)

In both retrievals, ε_{AD} generally becomes smaller as the temperature becomes warmer probably because the spectra have higher radiance and higher signal-to-noise ratio (SNR) in the sensitive altitude of 70–95 km. The sensitive altitude is described in “[Evaluation of the retrieval method](#)” section. (The effect of SNR was also evaluated by the model spectra with the white noise with the RMS intensity of 0.5 and 1.5 $\text{erg/s/cm}^2/\text{sr/cm}^{-1}$, shown in Additional file 1: Figure S1–S4. These noise levels are from the event study cases in “[Retrieval from the CO₂ absorption spectra observed by HIPWAC in May 2012](#)” section.)

In the following sections, we evaluate the retrieval results with the error of ε_{AD} estimated from one of the 5 model spectra whose radiance is closest to that of the observed spectrum.

Evaluation of the retrieval method

Accuracy of retrieval from model spectra

We evaluated the sensitive altitude regions and accuracies of the retrieved profiles in our retrieval using the model spectra generated from various temperature and wind velocity profiles as the emulated observed spectra. For this purpose, we generated 533 model spectra from the combination of 13 temperature profiles and 41 wind velocity profiles. The 13 temperature profiles were the VIRAex with the uniform bias between -30 K and $+30$ K with 5 K steps at all altitudes. The 41 wind velocity profiles were the uniform wind velocity from -200 m/s to $+200$ m/s with 10-m/s steps at all altitudes. For all cases, we also added white noise with the RMS of 1.0 $\text{erg/s/cm}^2/\text{sr/cm}^{-1}$. Hereafter, we refer to these assumed profiles as “true” values.

As for the a priori, we use the single profile fixed to VIRAex for the temperature and 0 m/s for the wind velocity in the following sections. As mentioned in “[Dependence on a priori profiles](#)” section, it is difficult to prepare appropriate a priori profiles for each observation because we do not have obtained enough characteristics of temperature and wind in Venusian mesosphere. Also, if we use different a priori profiles for different observed spectra, it becomes hard to distinguish whether the retrieved variations are due to actual phenomenon or dependence on a priori profile.

Figure 5 shows two model spectra as examples generated from the true temperature profiles of “VIRAex -30 K” (the cold case) and “VIRAex $+30$ K” (the warm

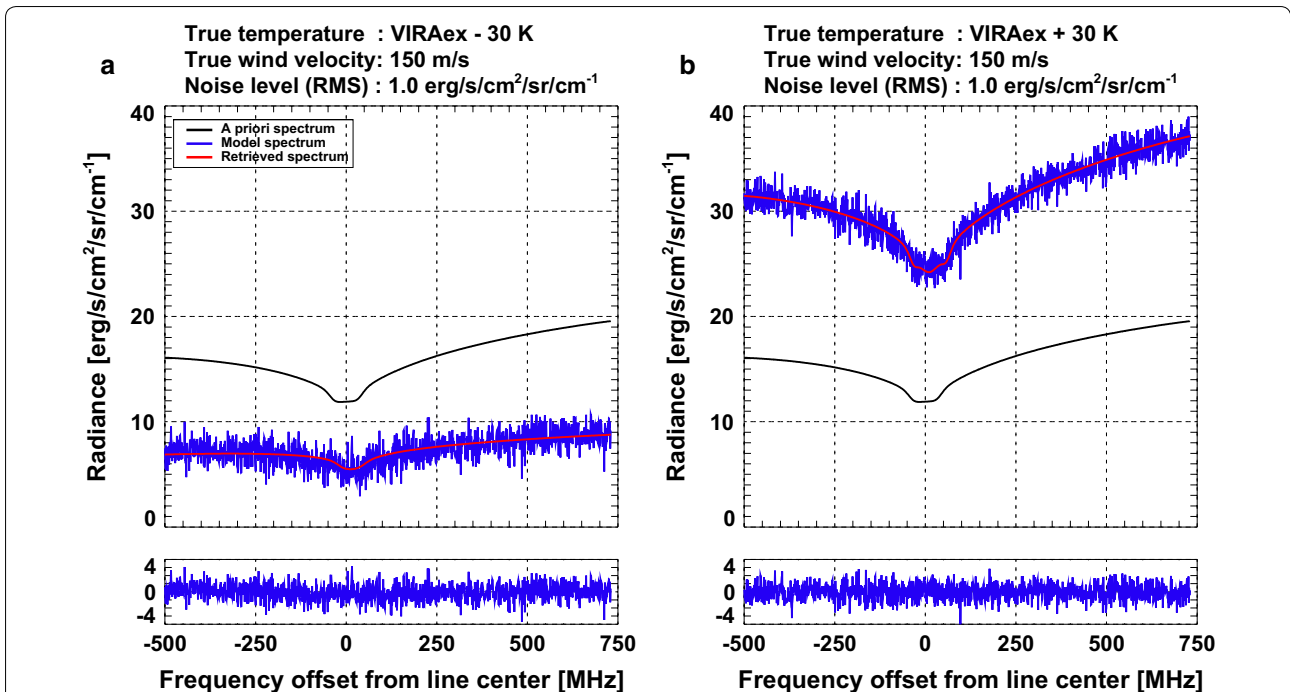


Fig. 5 Examples of the model spectra synthesized from the temperature profiles of **a** the cold case (VIRAex - 30 K) and **b** the warm case (VIRAex + 30 K). Upper panels show the model spectra (blue), a priori spectra (black), and retrieved spectra (red). Lower panels show the residuals between the model and retrieved spectra. Model spectra were generated with the wind velocity profile of + 150 m/s at all altitudes, including white noise with the RMS of 1.0 erg/s/cm²/sr/cm⁻¹. In both, the a priori profiles are VIRAex for the temperature and 0 m/s for the wind velocity at all altitudes

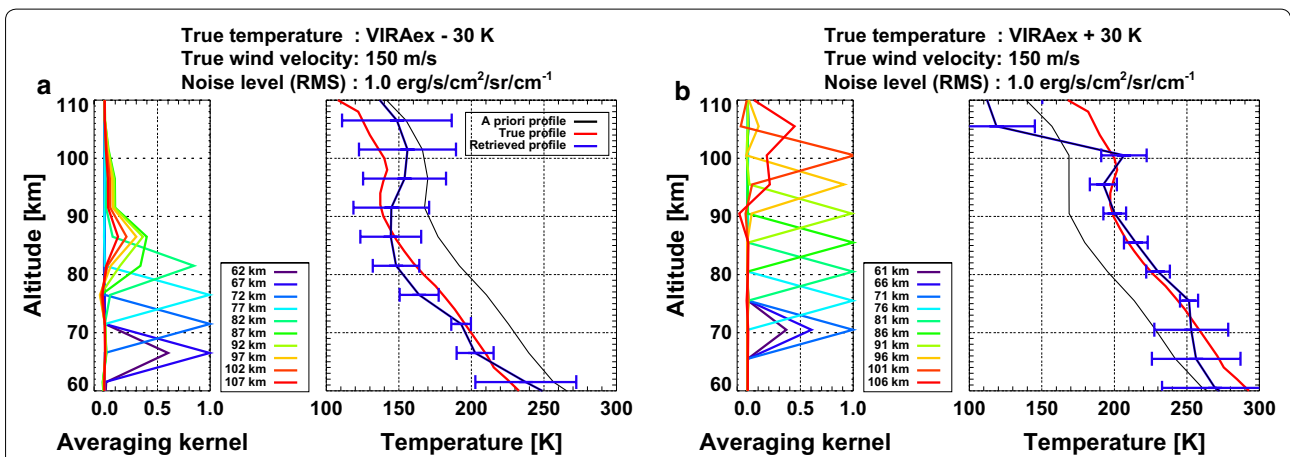


Fig. 6 Temperature profiles retrieved from the model spectra shown in Fig. 5. In the right panels of **a** and **b**, blue, red and black lines represent the retrieved, model, and a priori (VIRAex) profiles, respectively. Blue horizontal lines are the retrieval errors calculated using Eq. 1. Left panels of **a** and **b** show the averaging kernels (AKs). The peaks of AKs are the sensitive altitudes, and full-widths at half-maximum are their vertical resolutions

case). The true wind velocity profile was set as + 150 m/s at all altitudes for both spectra.

Figure 6 shows the temperature profiles of the retrieved spectra, corresponding to the red lines in Fig. 5 with their retrieval errors calculated from Eq. (1) and averaging

kernels (AKs). AK shows the altitudes where the retrieved values have sensitivities to true values. The full-width at half-maximum of AK also gives vertical resolution at each altitude. Deviations of the retrieved temperatures from the true profile are generally within the retrieval

errors, indicating that the retrieval error estimations are accurate. In the cold case, larger AK peaks were observed at the altitudes of 67–82 km. In the warm case, larger AK peaks were observed at the altitudes of 71–101 km. It is obvious that the warm case had a wider temperature retrieval range with a better precision because of a larger radiance level of the spectrum in the warm case.

The effect of the radiance level on the retrieval range is more evident in wind velocity retrieval. Figure 7 shows the wind velocity profiles of the retrieved spectra (red lines in Fig. 5) with their retrieval errors and AKs. The differences between the retrieved wind velocities and the true profile are within the retrieval errors. However, for the cold case, we cannot find a sensitive altitude with no evident AK peaks. In the warm case, the retrieved wind velocities in the 83–93 km range have large AK peaks close to 1.

Figure 8 shows the statistical results for the retrieved temperature (Fig. 8a, b) and wind velocity (Fig. 8c, d) profiles retrieved from the model spectra of 41 wind velocity profiles for the cold case (Fig. 8a, c) and the warm case (Fig. 8b, d). In Fig. 8, the standard deviations for the altitudes in the 60–100 km range were not larger than the mean retrieval errors in all cases. In particular, for the sensitive altitude regions with the AK close to 1, the standard deviations are close to the mean retrieval errors, and the true values are included within the mean retrieval errors at almost all the altitudes. These characteristics are also observed in the other temperature cases (VIRAex – 25 K ~ VIRAex + 25 K, not shown here). We concluded that the retrieval errors calculated using Eq. (1) can be used as retrieval accuracies.

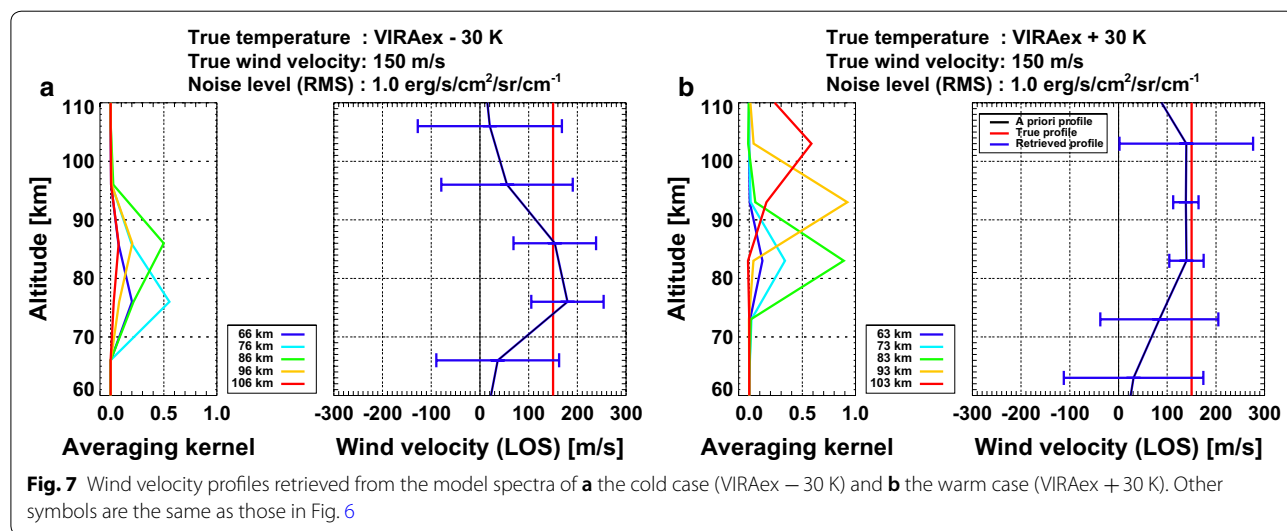
We note that there are some exceptions in the temperature retrieval. In Fig. 8a, the retrieved temperature

plus retrieval error at 72 km is slightly lower than the true value. In Fig. 8b, the retrieved temperature minus retrieval error at approximately 76 km is the same as the true value. In both cases, the retrieved temperature at the altitudes in the approximately 70–75 km range (close to the lower limit of the sensitive altitude region) appears to be affected by the large discrepancy between the retrieved and true profiles in the lower altitude region with insufficient sensitivity. Therefore, the retrieved temperature in the lower end of the sensitive altitude region should be treated carefully.

Figure 9 shows the mean errors in the retrieved temperature and wind velocity profiles from the model spectra with 41 wind velocity profiles in the cold, VIRAex, and warm cases. The errors for the intermediate temperature cases are between the errors of these cases (not shown here). Figure 9a shows that the temperature can be retrieved with the accuracy of ± 15 K at the altitudes of 70–75 km in the cold case, 70–95 km in the VIRAex case, and 75–100 km in the warm case. However, as shown in Fig. 9b, wind velocities can be retrieved with sufficient accuracy only for a limited range of altitudes. If accuracy worse than ± 50 m/s is unacceptable, wind velocity can only be retrieved at the altitude of 85 km for the VIRAex case and for the altitudes in the 85–95 km range for the warm case. We conclude that the wind velocity can be retrieved with the accuracy of ± 50 m/s for the 85–95 km altitude range in the ‘VIRAex – 20 K’ or higher temperature cases. For the ‘VIRAex – 25 K’ and ‘VIRAex – 30 K’ cases, the accuracies are worse than ± 50 m/s.

Effect of the noise level on the retrieval accuracies

In “Dependence on a priori profiles” and “Accuracy of retrieval from model spectra” sections, we evaluated our



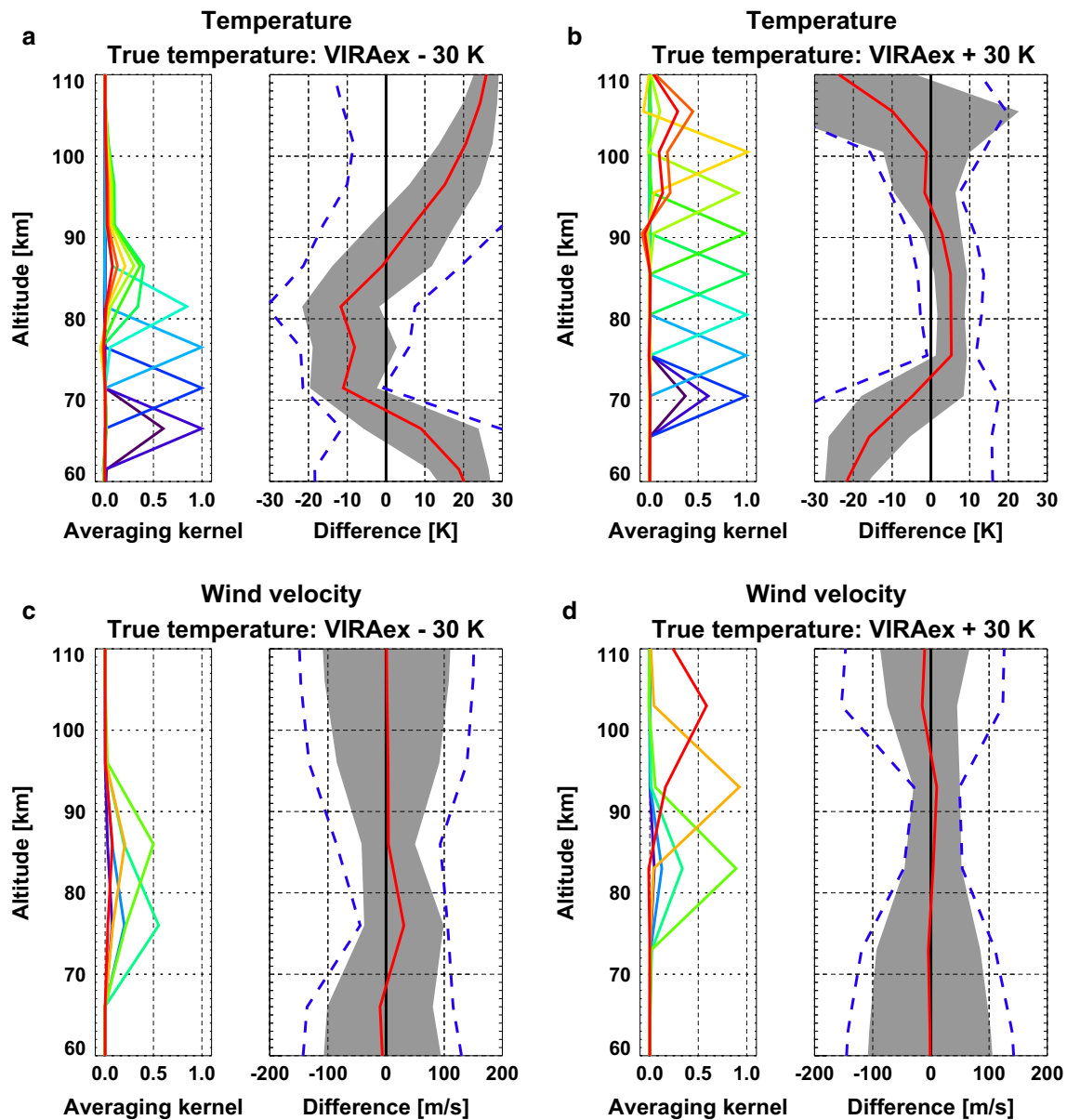


Fig. 8 Statistical results for **a, b** the retrieved temperatures and **c, d** wind velocities from the model spectra with 41 wind velocity profiles of -200 to $+200$ m/s at all altitudes and white noise with the RMS of $1.0 \text{ erg/s/cm}^2/\text{sr/cm}^{-1}$. The cold case results are shown in **a** and **c**, and the warm case results are shown in **b** and **d**. In the right panels of **a-d**, red lines are the mean differences between the retrieved and model profiles, gray areas are the standard deviations of the differences, and blue dashed lines are the mean retrieval errors. Left panels **a-d** show the same AKs in Figs. 6a, b, 7a, and b, respectively, as examples

retrieval tool for the observational data with the white noise with the RMS of $1.0 \text{ erg/s/cm}^2/\text{sr/cm}^{-1}$. We also evaluated the sensitive altitude regions and retrieval accuracy under two other noise cases, namely the RMS of $0.5 \text{ erg/s/cm}^2/\text{sr/cm}^{-1}$ (smaller noise level) and of $1.5 \text{ erg/s/cm}^2/\text{sr/cm}^{-1}$ (larger noise level). We applied these noise levels to the 533 model spectra, as shown in “Accuracy of retrieval from model spectra” section. Figure 10

shows the model spectra as examples generated from the temperature of VIRAEax and wind velocity of $+150$ m/s with smaller and larger noise levels, and the retrieved spectra. The a priori spectra with VIRAEax for the temperature and 0 m/s for all altitudes for the wind velocity are shown by black lines but overlap the retrieved spectra almost exactly.

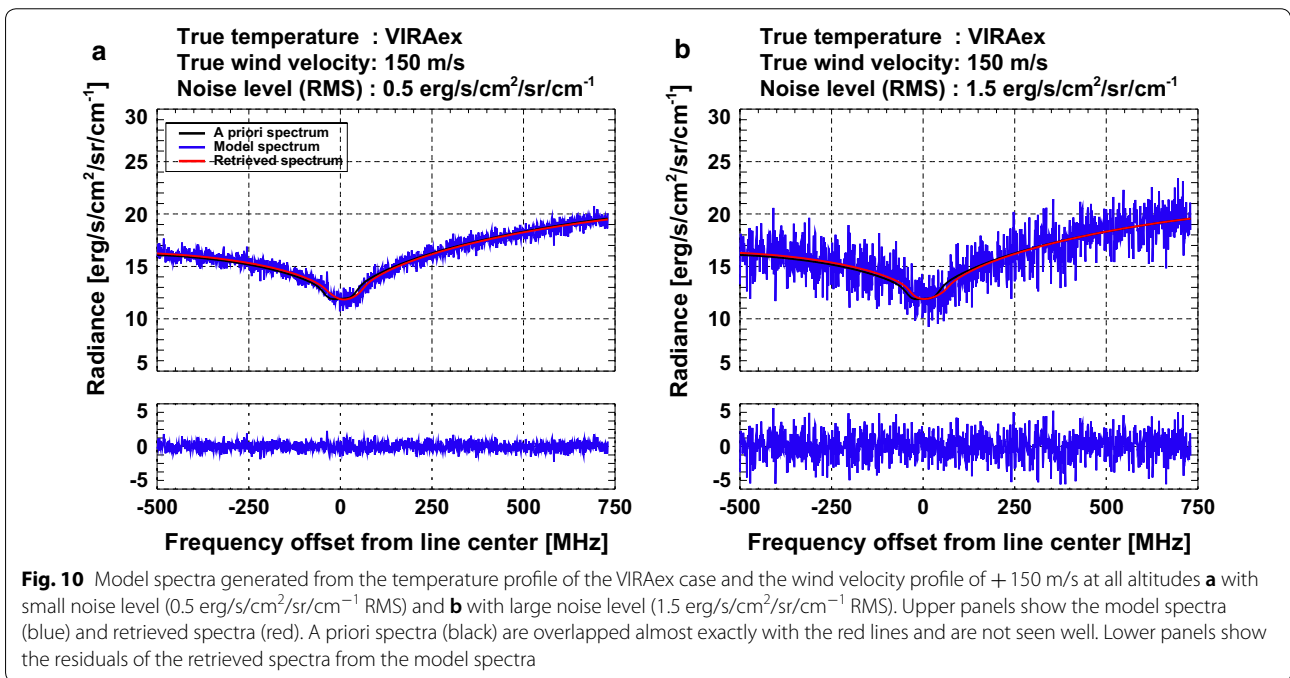
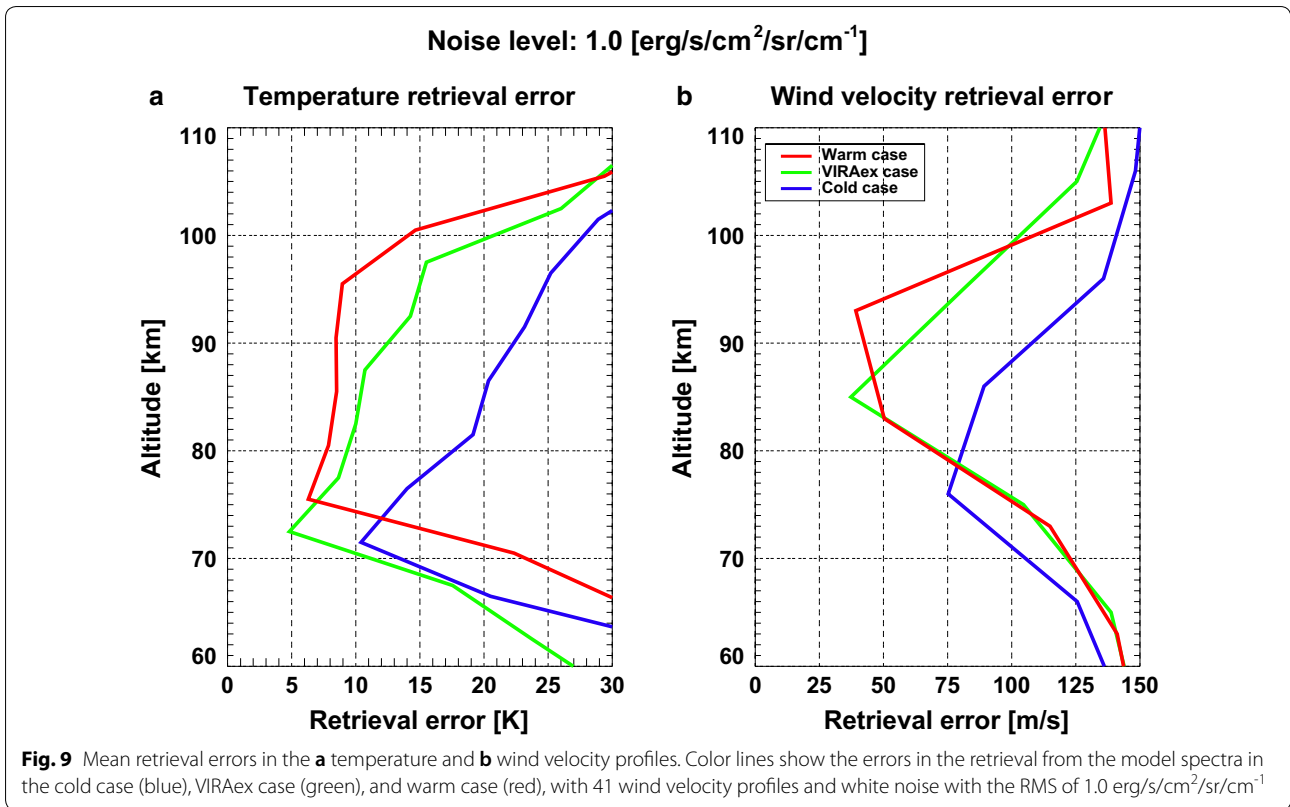
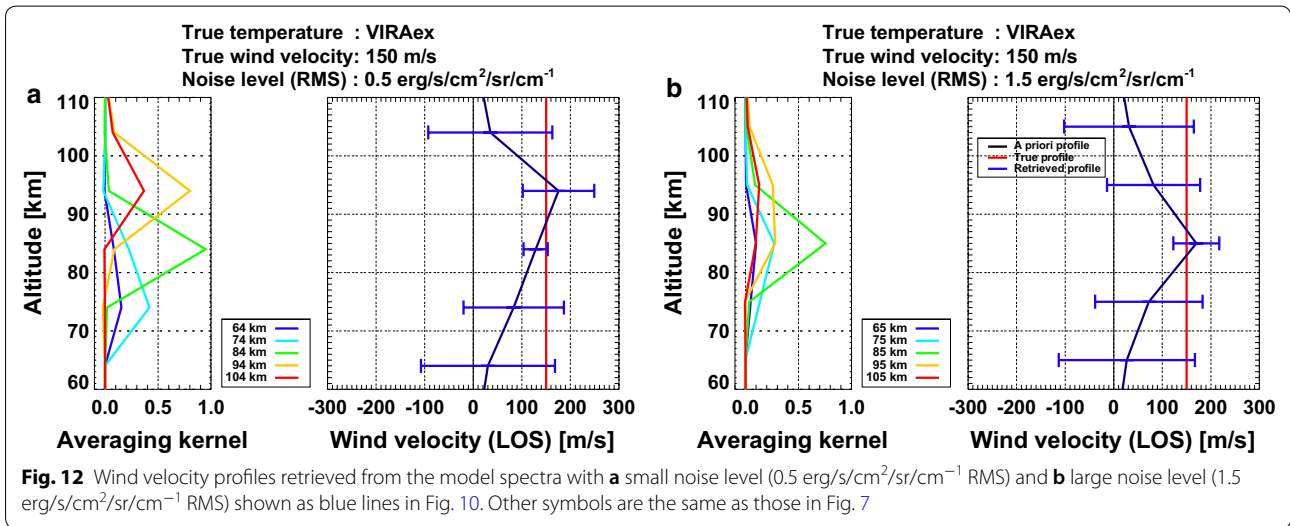
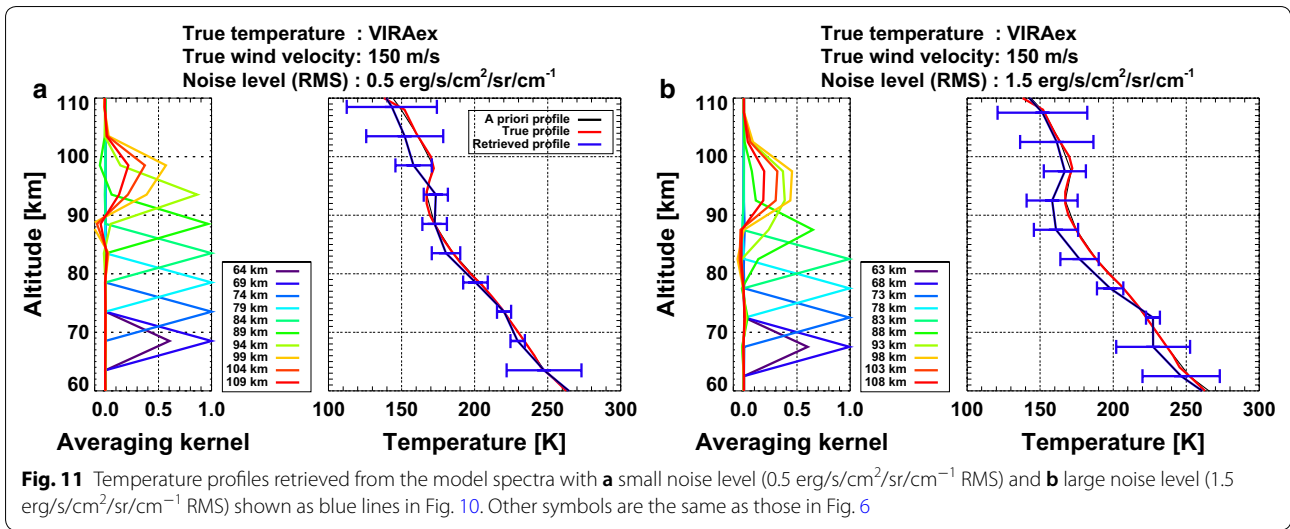


Figure 11 shows the temperature profiles retrieved from the spectra. In the smaller noise case, the upper limit altitude with the AK peak close to 1 is ~ 94 km, ~ 11 km

higher than that in the larger noise case (~ 83 km). In the larger noise case, the retrieval error becomes larger than 15 K at the lower limit altitude (~ 68 km). Figure 12 also

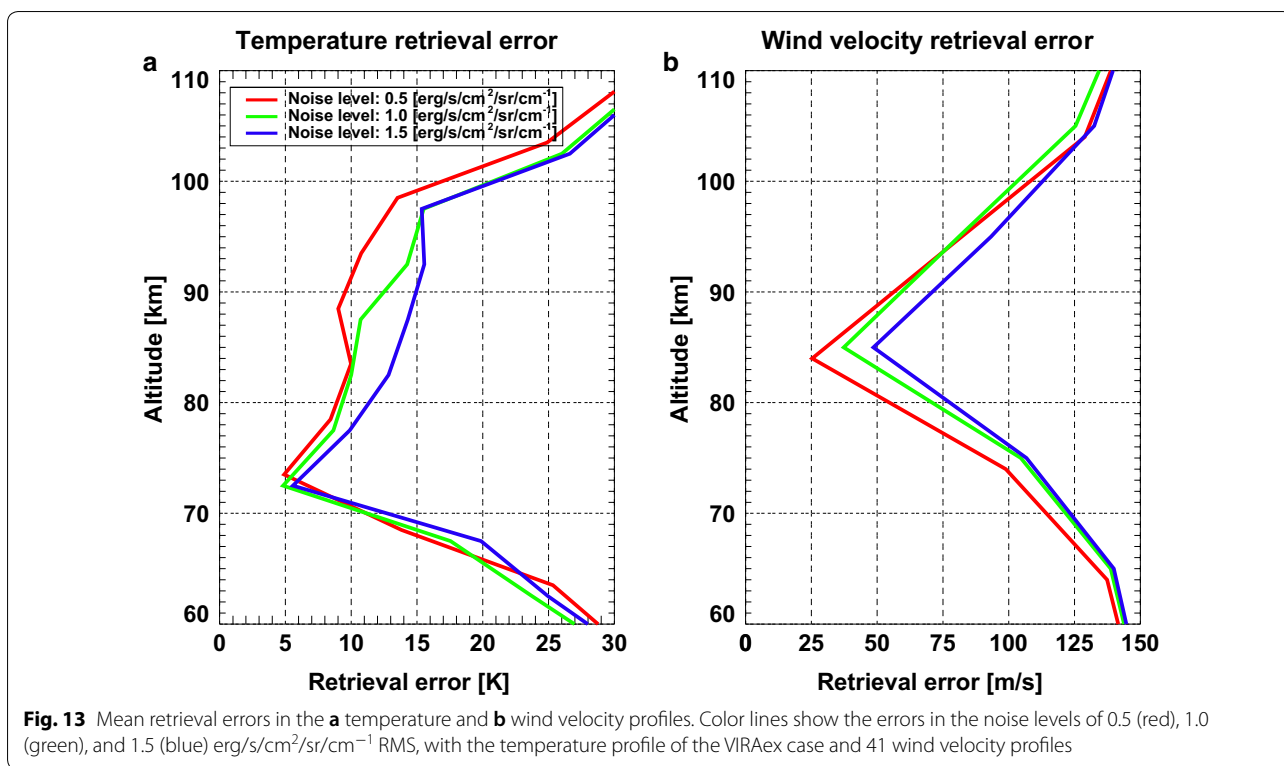


shows the wind velocity profiles retrieved from the model spectra shown in Fig. 10. In both cases, the retrieval results show the sensitivity at the altitude of approximately 85 km, with the retrieval error of ± 25 m/s in the smaller noise case and of ± 47 m/s in the larger noise case. In the smaller noise case, the AK peak is still high (~ 0.8) at the altitude of ~ 94 km but the retrieval error is ± 74 m/s.

Figure 13 shows the mean retrieval errors in the (a) temperature and (b) wind velocity profiles for the noise levels of 0.5, 1.0, and 1.5 erg/s/cm²/sr/cm⁻¹. The mean retrieval errors in the other temperature cases have similar characteristics (not shown here). In the temperature retrieval (Fig. 13a), the sensitive altitude regions with the accuracy of ± 15 K are 70–100 km, 70–95 km, and

70–90 km for retrieval with the RMS values of 0.5, 1.0, and 1.5 erg/s/cm²/sr/cm⁻¹, respectively. However, in the wind velocity retrieval (Fig. 13b), the retrieval accuracy at the most sensitive altitude of approximately 85 km was ± 25 m/s, ± 37 m/s, and ± 48 m/s for the noise levels of 0.5, 1.0, and 1.5 erg/s/cm²/sr/cm⁻¹, respectively. We conclude that the wind velocity at the altitude of approximately 85 km can be retrieved with the accuracy of better than ± 50 m/s when the noise level is 1.5 erg/s/cm²/sr/cm⁻¹ or less.

In this section, we have evaluated our method and its precision using synthetic spectra. Our retrieval method can obtain temperature profiles in the mesosphere above the cloud at altitudes 70–95 km with the vertical resolution of 5 km and the retrieval accuracy of ± 15 K from



the spectra of the temperature profile of VIRAx with the noise level of $1.0 \text{ erg/s/cm}^2/\text{sr/cm}^{-1}$. The retrieval accuracy can be improved and the upper boundary can be extended to 100 km by reducing the noise level. In addition, our retrieval method can obtain wind velocity at altitude 85–95 km with the vertical resolution of 10 km. The retrieval accuracy became better, changing from $\pm 50 \text{ m/s}$ for the noise levels of $1.5 \text{ erg/s/cm}^2/\text{sr/cm}^{-1}$ to $\pm 25 \text{ m/s}$ for the noise levels of $0.5 \text{ erg/s/cm}^2/\text{sr/cm}^{-1}$. Our result provides the first theoretical validation of the retrieval method for the wind velocity retrieval at this altitude range, which is important due to the lack of wind measurements in the same time frame, as mentioned below.

Retrieval from the CO₂ absorption spectra observed by HIPWAC in May 2012

The retrieved temperature and wind velocity profiles

We applied our retrieval method for real observation spectra from Venusian nightside CO₂ absorption line profiles obtained by a mid-infrared heterodyne spectrometer. This event study used the data obtained by HIPWAC attached to NASA/IRTF 3-m telescope on May 19–22, 2012. The dataset was originally analyzed and published by Staingier et al. (2015), and can be used to assess the validity of our retrieval scheme.

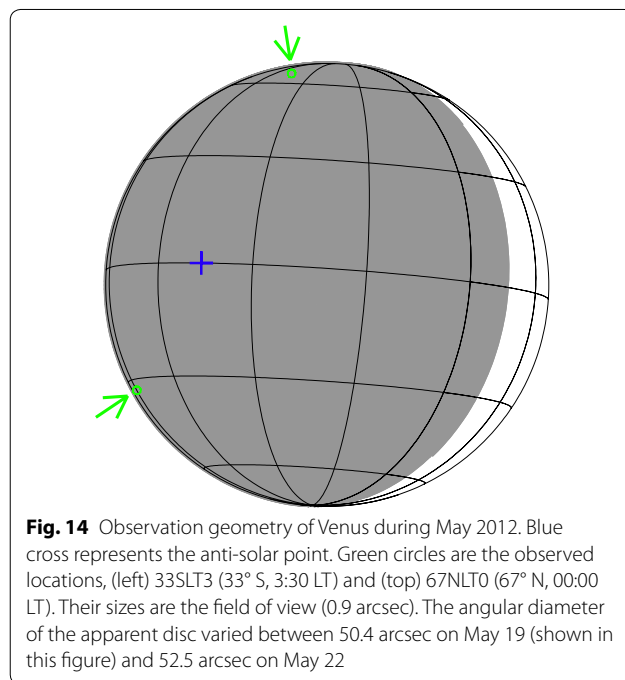
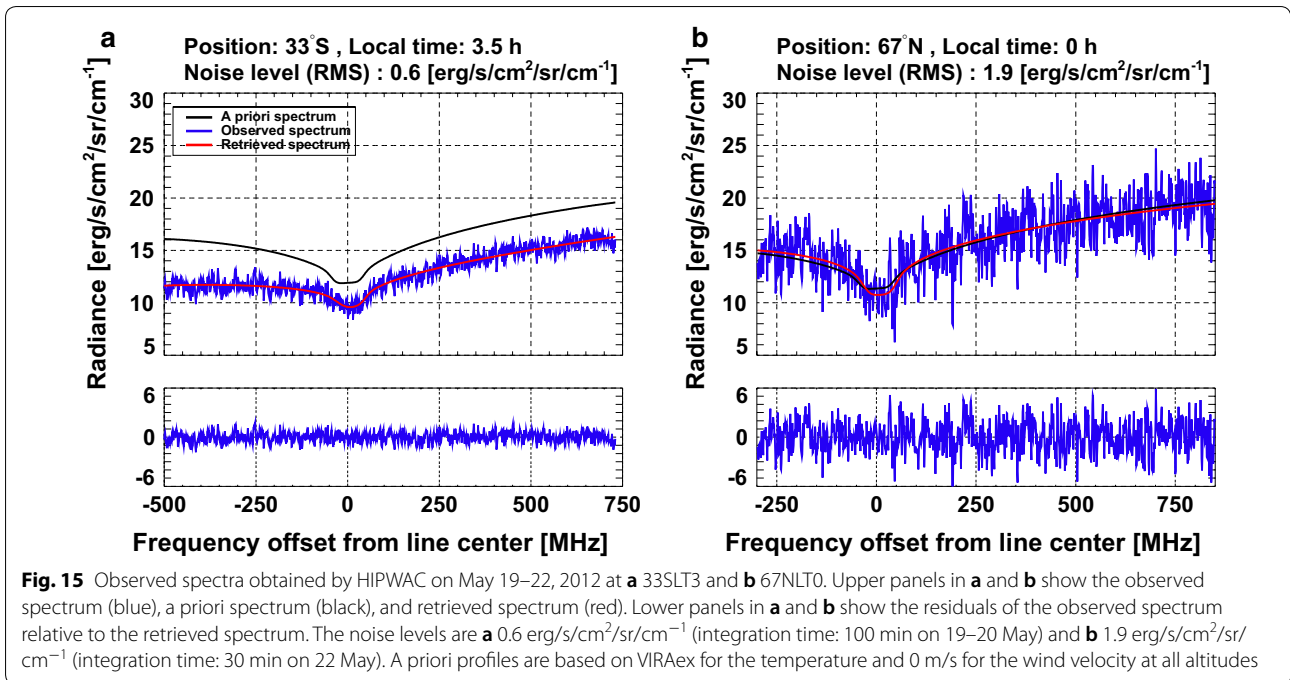


Figure 14 shows the observation geometry with the apparent illumination of Venus disk. The data were obtained at two points, namely at 33° S latitude and local time (LT) of 03:30 (hereafter, 33SLT3) and at 67° N

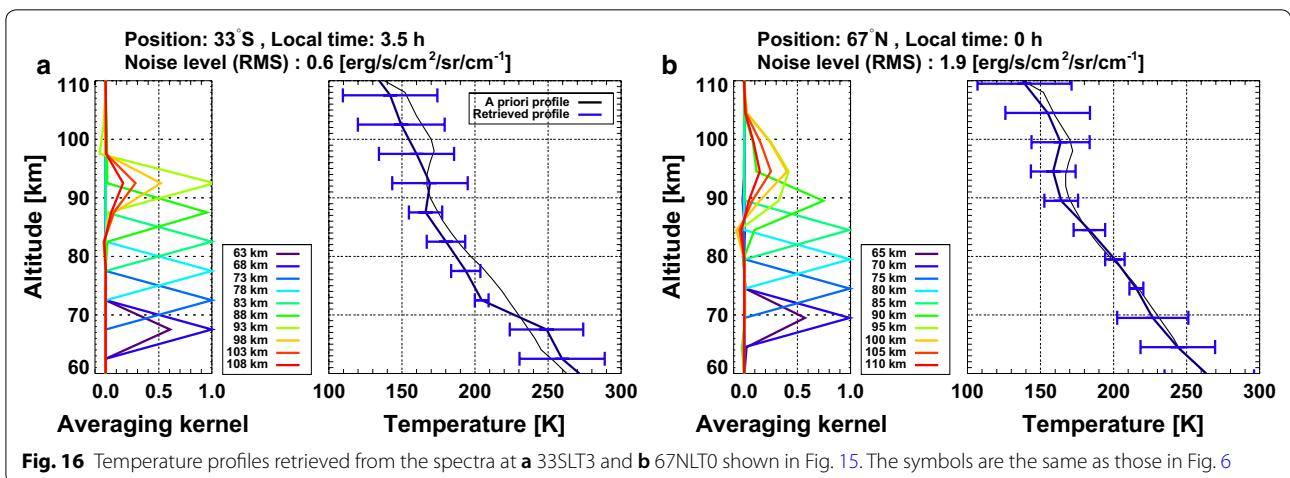


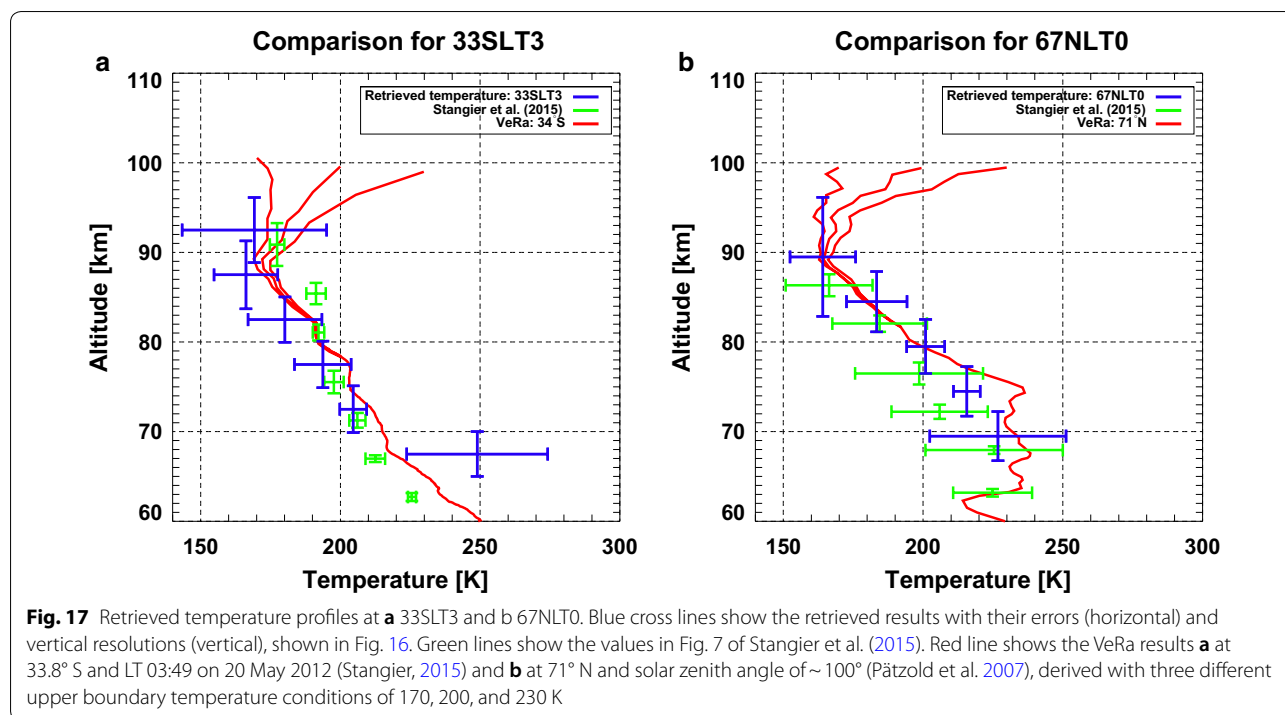
latitude and 00:00 LT (hereafter, 67NLT0). The field of view of HIPWAC was 0.9 arcsec on the Venusian apparent angular diameter of 50.4 arcsec on May 19, 2012 and 52.5 arcsec on May 22, 2012.

Figure 15 shows the observed spectra after binning the data with 1 MHz obtained at 33SLT3 with the integration time of 100 min on source on May 19–20, 2012 and at 67NLT0 with the integration time of 30 min on source on May 22, 2012. The RMS noise at 33SLT3 (~ 0.6 erg/s/cm²/sr/cm⁻¹) was three times smaller than that at 67NLT0 (~ 1.9 erg/s/cm²/sr/cm⁻¹) mostly due to its longer integration time. We also note that the mean background

radiance at 33SLT3 (~ 14.6 erg/s/cm²/sr/cm⁻¹) is $\sim 25\%$ smaller than that at 67NLT0 (~ 19.5 erg/s/cm²/sr/cm⁻¹).

Figure 16 shows our retrieved temperature profiles for (a) 33SLT3 and (b) 67NLT0, respectively. The retrieved temperature profiles had sensitivity at the altitudes in the 68–93 km range at 33SLT3 and in the 70–90 km range at 67NLT0, respectively, by judging from the peak value of Aks. The uncertainties of the retrieved temperature profile were less than ~ 13 K at the sensitive altitudes of 73–88 km at 33SLT3 and 75–90 km at 67NLT0. These results are in good agreement with the results described in “Evaluation of the retrieval method” section of this paper and in Fig. 9 of Nakagawa et al. (2016). We note





that larger uncertainties (~ 26 K) are found in the vicinity of the lower and upper boundaries of the sensitivity region, at ~ 68 km and ~ 93 km at 33SLT3 and at ~ 70 km at 67NLT0.

Figure 17 compares our results to the temperature profiles shown in Fig. 7 of Stangier et al. (2015) and to the previously obtained results in order to validate our retrieval tool. Figure 17a compares the retrieved temperature profiles at 33SLT3 with the values retrieved by Stangier et al. (2015). The values derived from VEX Radio Science (VeRa) radio occultation measurements at 33.8° S and 3:49 LT on 20 May 2012 (Stangier, 2015) are also shown in Fig. 17a. The three VeRa profiles have different upper boundary temperatures of 170, 200, and 230 K, respectively. Our results show a good agreement with both temperature profiles of Stangier et al. (2015) and VeRa (except for the altitudes of approximately 68 km and 88 km of Stangier et al. (2015)) and support a gradual temperature decrease at the altitudes from 70 to 90 km. As shown in Fig. 17b, the retrieved temperature at 67NLT0 is also in agreement with the results of Stangier et al. (2015) within the retrieval errors. Figure 17b also presents the temperature profile derived from VEX VeRa obtained at 71° N in 2006 (Pätzold et al. 2007). The gradual temperature decreases at the altitudes from 75 to 90 km are observed for both sets of results. The excellent agreement of temperatures with previous retrieval results provides a good validation of the technique for temperatures.

Figure 18 shows the retrieved wind profiles with the Aks at (a) 33SLT3 and (b) 67NLT0. The retrieved results show that the observed CO_2 absorption line profiles are sensitive to the wind velocity at the altitudes of 84 ± 6 and 94 ± 7 km at 33SLT3 and 80 ± 7 and 90 ± 7 km at 67NLT0 in agreement with the results described in “Evaluation of the retrieval method” section above and in Fig. 11 of Nakagawa et al. (2016). The retrieved results at 33SLT3 are $+35 \pm 28$ m/s at 84 ± 6 km and $+144 \pm 70$ m/s at the altitude of 94 ± 7 km, corresponding to the SS-AS flows at both altitudes. This result is unexpected because it is in the opposite direction of the RSZ wind at the cloud top altitude (~ 70 km). Meanwhile, the retrieved wind velocity at 67NLT0 was 66 ± 73 m/s at 80 ± 7 km and 112 ± 69 m/s at 90 ± 7 km, indicating the potential meridional circulation toward the equator at both altitudes. Retrieval accuracy of ± 28 m/s at 84 ± 6 km at 33SLT3 could satisfy our requirement of ± 50 m/s. The other retrieval accuracies at 94 ± 7 km at 33SLT3, and 80 ± 7 and 90 ± 7 km at 67NLT0 show less sensitive, although the Aks at these altitudes are rather than 0.6. In contrast to temperatures, we have to admit that the wind validation is more difficult due to the lack of wind measurements in the same time frame or location. The newly retrieved winds in this study are compared to previous theoretical models in the next subsection.

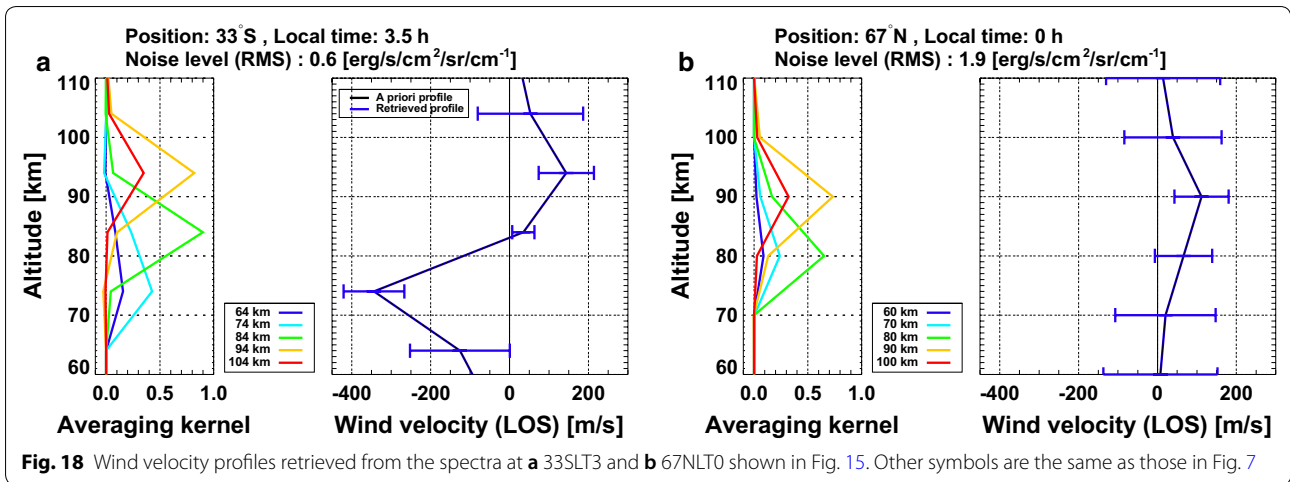


Fig. 18 Wind velocity profiles retrieved from the spectra at **a** 33SLT3 and **b** 67NLT0 shown in Fig. 15. Other symbols are the same as those in Fig. 7

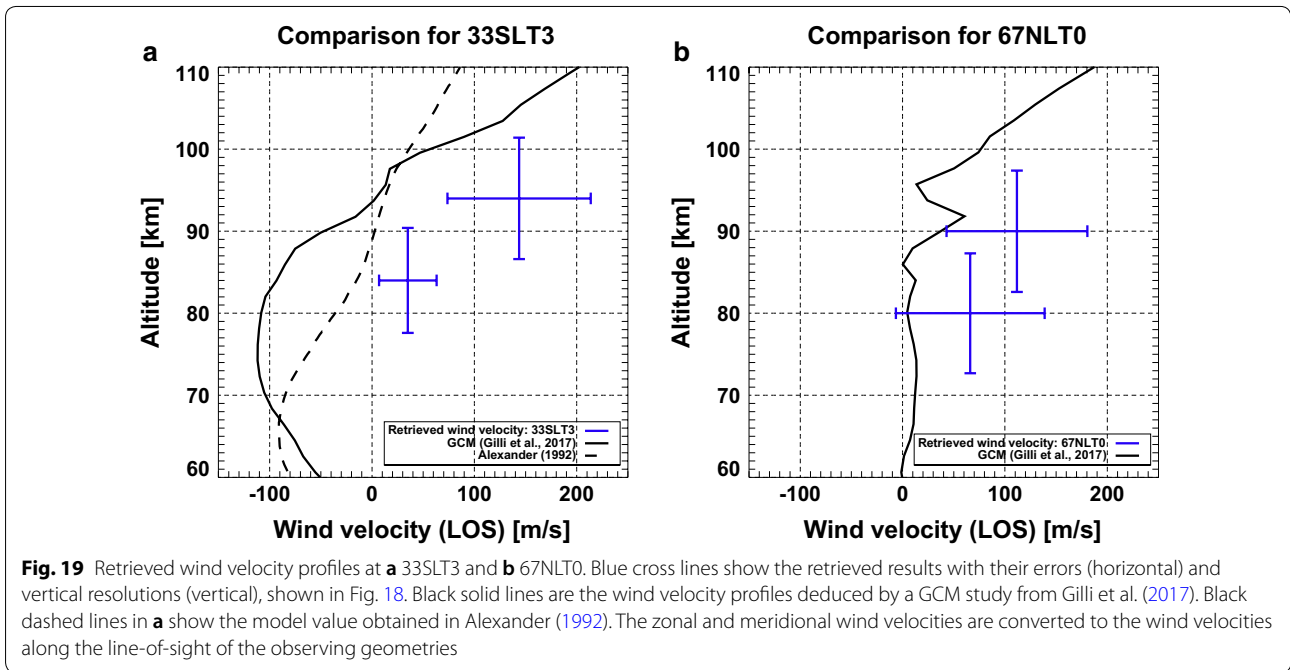


Fig. 19 Retrieved wind velocity profiles at **a** 33SLT3 and **b** 67NLT0. Blue cross lines show the retrieved results with their errors (horizontal) and vertical resolutions (vertical), shown in Fig. 18. Black solid lines are the wind velocity profiles deduced by a GCM study from Gilli et al. (2017). Black dashed lines in **a** show the model value obtained in Alexander (1992). The zonal and meridional wind velocities are converted to the wind velocities along the line-of-sight of the observing geometries

Discussion of wind in the mesosphere

Figure 19 shows the retrieved wind velocity profiles at (a) 33SLT3 and (b) 67NLT0 in comparison with two numerical models by Gilli et al. (2017) for 33SLT3, and 67NLT0 and by Alexander (1992) for 33SLT3. The numerical simulation by Gilli et al. (2017) which is a full self-consistent Venus GCM has addressed physical and photochemical processes at region of ground-to-thermosphere. This model included a new non-orographic GW parameterization to describe the dynamical effects in the upper mesosphere/lower thermosphere, which is good for comparison with the retrieved wind in this study. In addition, the wind velocity profile of

Alexander (1992) is controlled by gravity waves that propagate from the middle atmosphere via momentum deposition in the upper atmosphere, driving wave-induced accelerations in the thermosphere. For the comparison, all of the wind velocities shown in Fig. 19 are converted to the along line-of-sight velocities in the same geometry as that in our analyses as shown in Fig. 14.

If we assume the presence of either pure SS-AS flow or pure RSZ wind field, the SS-AS flow yields positive Doppler wind direction at 33SLT3 (eastward wind) while the RSZ wind (westward wind) should appear as negative Doppler wind direction.

Our results added the information for the wind velocities at the altitudes of 84–94 km that showed larger SS-AS flow velocity values than those of the previous observations. In the numerical results of this region in the study by Alexander (1992) and in a GCM study from Gilli et al. (2017), the transition altitude from the RSZ wind to the SS-AS flow is observed at approximately 90 km and wind velocity gradually increases at higher altitudes. Our results suggested that this transient can be shifted to altitudes lower than 90 km.

At 67NLT0, positive Doppler wind velocity (the equatorward movement) can be interpreted as SS-AS flow. The wind found in the GCM study from Gilli et al. (2017) shows the positive wind velocity at the altitudes above 65 km. Our retrieved results are in agreement with the results of this model within the retrieval error margins.

Our results are the first direct wind measurements of the Venusian mesosphere at the altitudes of 85–95 km, and showed a further weakening of the RSZ wind. Although the number of observation points was limited, the retrieved Doppler wind velocity profiles make us think of the presence of SS-AS flow in the altitude of 85–95 km which has never been explained. It is noteworthy that a decrease of the RSZ wind in the mesosphere between the cloud top and 80 km was also observed as thermal winds derived by recent measurement of VIRTIS-M on the nightside (Peralta et al. 2017). At the altitudes, the internal GWs propagating upward may deposit their horizontal momentum into the background mean winds and change the mean wind velocity (Hoshino et al. 2013; Nakagawa et al. 2013). It is noteworthy that a potential convective instability layer was observed by radio occultation measurements by Akatsuki at the altitude around 80–90 km (Imamura et al. 2017). However, we should also note that the wave breaking altitude predicted by GCM, ~ 130 km, was much higher (Hoshino et al. 2013; Nakagawa et al. 2013) than the 85–95 km region. Further investigations are crucial for identifying the transition region from RSZ wind to SS-AS flow.

Another possible explanation for the unexpected strong SS-AS flow at 85–95 km is the advection flow due to improved IR heating and an additional aerosol heating in the dayside atmosphere. A previous GCM study found much lower temperatures than those observed by VEX SOIR, obtaining -50 K at the altitudes of 85–100 km at the terminator (Bougher et al. 2015); it was claimed that

therefore there should be some mechanisms for the heating of the dayside atmosphere. If the dayside atmosphere is additionally heated, the SS-AS flow in the mesosphere will be enhanced. Therefore, further wind distribution information is required to establish appropriate atmospheric waves and heating models. The discovery of an unexpected SS-AS flow at the altitude of 85–95 km would affect our understanding of the Venusian mesosphere.

Summary

We have evaluated a method to retrieve temperature and Doppler wind velocity profiles from CO₂ absorption line profiles observed with mid-infrared heterodyne spectroscopy. Based on the errors originating from uncertainties in the a priori profiles, we estimated the achievable sensitive altitude and retrieval accuracy using model spectra generated from various temperature and wind profiles with different noise levels. The evaluation suggested that the temperature profiles can be retrieved at altitudes in the 70–95 km range with a vertical resolution of 5 km and retrieval accuracy of ± 15 K by retrieving model spectra with a temperature profile as given by VIRA (Seiff et al. 1985) and Seiff and Kirk (1982). The assumed nominal noise level was $1.0 \text{ erg/s/cm}^2/\text{sr/cm}^{-1}$. For data with a higher signal-to-noise ratio (higher radiance and/or lower noise level), the retrieval accuracy can be improved and the upper boundary can be extended to 100 km. By contrast, the wind velocity profile was more difficult to obtain but still could be retrieved at an altitude of approximately 85 km with a vertical resolution of 10 km. For data with a higher signal-to-noise ratio, the retrieval accuracy became better, changing from ± 50 m/s for noise levels of $1.5 \text{ erg/s/cm}^2/\text{sr/cm}^{-1}$ to ± 25 m/s for noise levels of $0.5 \text{ erg/s/cm}^2/\text{sr/cm}^{-1}$. The sensitive altitude could also be improved. This result provides the first validation of a method for wind velocity retrieval in the Venusian mesosphere at altitudes of 85–95 km.

We applied our retrieval method using the spectra obtained by HIPWAC observations in May 2012 with data partially in common with the study by Stangier et al. (2015). We confirmed that the retrieved temperature profiles were in good agreement with the results of Stangier et al. (2015) and Pätzold et al. (2007), validating our method. At last, we retrieved the wind velocity at the altitudes of 80–95 km, and showed that the wind velocity at 33° S and 3 LT represented the SS-AS flow at altitudes of 84 ± 6 km and 94 ± 7 km. We also retrieved the wind velocity at 67° N and 0 LT as the meridional circulation

toward the equator at the altitudes of 80 ± 7 km and 90 ± 7 km. These velocities were consistent with the wind profile obtained by GCM of Gilli et al. (2017), but the retrieved wind at 33° S was stronger. Our results suggested that the transition region between the RSZ wind and SS-AS flow is found lower than 90 km which had been predicted to be the transition altitude.

Our result is an event study, and does not conclusively resolve whether these mesospheric flows were ‘sporadic and patchy’ or ‘permanent and large’ features. For further observations, we will utilize our mid-infrared heterodyne spectrometer MILAHI (Nakagawa et al. 2016) attached to the Tohoku University 60-cm telescope at the summit of Haleakalā, Hawaii.

Supplementary information

Supplementary information accompanies this paper at <https://doi.org/10.1186/s40623-020-01188-0>.

Additional file 1. Figure S1. Five model spectra including white noise with the RMS of $0.5 \text{ erg/s/cm}^2/\text{sr/cm}^{-1}$. Other symbols are the same as those in Fig. 1. **Figure S2.** Standard deviations for the (a) temperature and (b) wind velocity in the retrieval results from the five model spectra shown in Figure S1. Other symbols are the same as those in Fig. 4. **Figure S3.** Five model spectra including white noise with the RMS of $1.5 \text{ erg/s/cm}^2/\text{sr/cm}^{-1}$. Other symbols are the same as those in Fig. 1. **Figure S4.** Standard deviations for the (a) temperature and (b) wind velocity in the retrieval results from the five model spectra shown in Figure S3. Other symbols are the same as those in Fig. 4.

Abbreviations

AK: Averaging kernel; AMATERASU: Advanced Model for Atmospheric TeraHertz Radiation Analysis and Simulation; GCM: General circulation model; IPLS/LMD: Institut Pierre Simon Laplace/Laboratoire de Météorologie Dynamique; GW: Gravity wave; HIPWAC: Heterodyne Instrument for Planetary Wind and Composition; IRTF: InfraRed Telescope Facility; LT: Local time; LTE: Local thermodynamic equilibrium; MILAHI: Mid-Infrared LAsER Heterodyne Instrument; NASA: National Aeronautics and Space Administration; RMS: Root mean square; RSZ: Retrograde superrotational zonal; SNR: Signal-to-noise ratio; SOIR: Solar Occultation at InfraRed; SPICAV: Spectroscopy for the Investigation of the Characteristics of the Atmosphere of Venus; SS-AS: Subsolar-to-antisolar; VEX: Venus Express; VIRA: Venus International Reference Atmosphere; VIRTIS: Visible and InfraRed Thermal Imaging Spectrometer; VMC: Venus Monitoring Camera; VeRa: Venus Express Radio Science.

Acknowledgements

This work was carried out by the international joint research program of the Institute for Space-Earth Environmental Research, Nagoya University, and the Payload Basic Development Program of Institute of Space and Astronautical Science, Japan Aerospace and Exploration Agency. GG work was supported by Fundação para a Ciência e a Tecnologia (FCT) through the research grants UIDB/04434/2020, UIDP/04434/2020, P-TUGA PTDC/FIS-AST/29942/2017, and by the European Union’s Horizon2020 research and innovation programme under the Marie Skłodowska-Curie grant agreement No 796923.

Authors’ contributions

KT is the lead author of this article and has the overall responsibility for the results presented in this paper. HN is the collaborator supporting the analyses of the data obtained using the heterodyne spectrometer. HS is the collaborator supporting the retrieval tool evaluations. PK is the collaborator supporting the data analyses of the heterodyne spectrometer. IM is the collaborator supporting the analyses of the data obtained using the heterodyne spectrometer. He is also the supervisor of the Ph.D. thesis of KT. YK is the

collaborator supporting the overall studies and funding for the work summarized in this paper. He is also the vice supervisor of the Ph.D. thesis of KT. TK is the collaborator supporting the discussions linked to the modeling studies. SA is the collaborator supporting the analyses of the data obtained using the heterodyne spectrometer and discussions linked to the Venus Express data. TK is the collaborator supporting the discussions linked to the Venus Express data. TK and TAL are the collaborators providing the HIPWAC observation data and supporting the data analyses of this instrument. GG is the collaborator supporting the modeling studies. All authors read and approved the final manuscript.

Funding

This work was supported by the Japan Society for the Promotion of Science (JSPS) Grants-in-Aid for Scientific Research (16H02231, 19H00707).

Availability of data and materials

The original raw data observed by the HIPWAC instrument are provided from NASA/GSFC (T. Kostiuk and T.A. Livengood). The datasets used and/or analyzed during the current study are available from the corresponding author on reasonable request.

Competing interests

The authors declare that they have no competing interests.

Author details

¹ Department of Geophysics, Graduate School of Science, Tohoku University, Aramaki-aza-Aoba 6-3, Aoba, Sendai, Miyagi 980-8578, Japan. ² Faculty of Science, Kyoto Sangyo University, Kamigamo, Kita-ku, Motoyama, Kyoto 603-8555, Japan. ³ Physical Institute, Universität zu Köln, Cologne, Germany. ⁴ Graduate School of Environmental Studies, Tohoku University, Sendai, Miyagi 980-8578, Japan. ⁵ Planetary Plasma and Atmospheric Research Center, Graduate School of Science, Tohoku University, Sendai, Miyagi 980-8578, Japan. ⁶ Planetary Aeronomy, Belgian Institute for Space Aeronomy, 3 av. Circulaire, 1180 Brussels, Belgium. ⁷ LPAP, STAR Institute, Université de Liège, Liège, Belgium. ⁸ Artificial Intelligence Research Center, National Institute of Advanced Industrial Science and Technology, 2-3-26 Aomi, Koto-ku, Tokyo 135-0064, Japan. ⁹ NASA Goddard Space Flight Center, Code 693, Greenbelt, MD 20771, USA. ¹⁰ Instituto de Astrofísica e Ciências do Espaço (IA), Tapada da Ajuda, Edifício Leste-2 piso, 1349-018 Lisbon, Portugal.

Received: 21 January 2020 Accepted: 25 April 2020

Published online: 07 May 2020

References

- Alexander MJ (1992) A mechanism for the Venus thermospheric superrotation. *Geophys Res Lett* 19:2207–2210. <https://doi.org/10.1029/92GL02110>
- Ando H, Takagi M, Fukuhara T, Imamura T, Sugimoto N, Sagawa H, Noguchi K, Tellmann S, Pätzold M, Häusler B, Murata Y, Takeuchi H, Yamazaki A, Toda T, Tomiki A, Choudhary R, Kumar K, Ramkumar G, Antonita M (2018) Local time dependence of the thermal structure in the Venusian equatorial upper atmosphere: comparison of Akatsuki radio occultation measurements and GCM results. *J Geophys Res Planets* 123:2270–2280. <https://doi.org/10.1029/2018JE005640>
- Baron P, Mendrok J, Kasai Y, Ochiai S, Seta T, Sagi K, Suzuki K, Sagawa H, Urban J (2008) AMATERASU: Model for Atmospheric TeraHertz Radiation Analysis and Simulation, *J Natl Inst Info Commun Technol* 55(1):109–121. <http://www.nict.go.jp/publication/shuppan/kihou-journal/journal-vol55-no1/07-04.pdf>
- Baron P, Urban J, Sagawa H, Möller J, Murtagh DP, Mendrok J, Dupuy E, Sato TO, Ochiai S, Suzuki K, Manabe T, Nishibori T, Kikuchi K, Sato R, Takayanagi M, Murayama Y, Shiotani M, Kasai Y (2011) The Level 2 research product algorithms for the Superconducting Submillimeter-Wave Limb-Emission Sounder (SMILES). *Atmos Meas Tech* 4:2105–2124. <https://doi.org/10.5194/amt-4-2105-2011>
- Bertaux JL, Vandaele AC, Korabiev O, Villard E, Fedorova A, Fussen D, Quémerais E, Belyaev D, Mahieux A, Montmessin F, Muller C, Neefs E, Nevejans D, Wilquet V, Dubois JP, Hauchecorne A, Stepanov A, Vinogradov I, Rodin AV, the SPICAV, SOIR team (2007) A warm layer in Venus’ cryosphere

- and high-altitude measurements of HF, HCl, H₂O and HDO. *Nature* 450:646–649. <https://doi.org/10.1038/nature05974>
- Bougher SW, Rafkin S, Drossart P (2006) Dynamics of the Venus upper atmosphere: outstanding problems and new constraints expected from Venus Express. *Planet Space Sci* 54:1371–1380. <https://doi.org/10.1016/j.pss.2006.04.23>
- Bougher SW, Brecht AS, Schulte R, Fischer J, Parkinson CD, Mahieux A, Wilquet V, Vandaele A (2015) Upper atmosphere temperature structure at the Venusian terminators: a comparison of SOIR and VTGCM results. *Planet Space Sci* 113:336–346. <https://doi.org/10.1016/j.pss.2015.01.012>
- Clancy RT, Sandor BJ, Moriarty-Schieven G (2012a) Thermal structure and CO distribution for the Venus mesosphere/lower thermosphere: 2001–2009 inferior conjunction sub-millimeter CO absorption line observations. *Icarus* 217:779–793. <https://doi.org/10.1016/j.icarus.2011.05.032>
- Clancy RT, Sandor BJ, Moriarty-Schieven G (2012b) Circulation of the Venus upper mesosphere/lower thermosphere: Doppler wind measurements from 2001–2009 inferior conjunction, sub-millimeter CO absorption line observations. *Icarus* 217:794–812. <https://doi.org/10.1016/j.icarus.2011.05.021>
- Clancy RT, Sandor BJ, Hoge J (2015) Doppler winds mapped around the lower thermospheric terminator of Venus: 2012 solar transit observations from the James Clerk Maxwell Telescope. *Icarus* 254:233–258. <https://doi.org/10.1016/j.icarus.2015.03.031>
- Drossart P, Piccioni G, Gérard J, Lopez-Valverde MA, Sanchez-Lavega A, Zasova L, Hueso R, Taylor FW, Bézard B, Adriani A, Angrilli F, Arnold G, Baines KH, Bellucci G, Benkhoff J, Bibring JP, Blanco A, Blecka M, Carlson RW, Coradini A, Di Lellis A, Encrenaz T, Erard S, Fonti S, Formisano V, Fouchet T, Garcia R, Haus R, Helbert J, Ignatiev NI, Irwin P, Langevin Y, Lebonnois S, Luz D, Marinangeli L, Orofino V, Rodin AV, Roos-Serote MC, Saggion B, Stam DM, Titov D, Visconti G, Zambelli M, Tsang C, the VIRTIS-Venus Express Technical Team (2007) A dynamic upper atmosphere of Venus as revealed by VIRTIS on Venus Express. *Nature* 450:641–645. <https://doi.org/10.1038/nature06140>
- Eymet V, Fournier R, Dufresne JL, Lebonnois S, Hourdin F, Bullock MA (2009) Net exchange parameterization of thermal infrared radiative transfer in Venus' atmosphere. *J Geophys Res* 114:E11008. <https://doi.org/10.1029/2008JE003276>
- Gérard JC, Bougher SW, Lopez-Valverde MA, Patzold M, Drossart P, Piccioni G (2017) Aeronomy of the Venus upper atmosphere. *Space Sci Rev* 212:1617–1683. <https://doi.org/10.1007/s11214-017-0422-0>
- Gilli G, Lebonnois S, González-Galindo F, López-Valverde MA, Stolzenbach A, Lefèvre F, Chaufray JY, Lott F (2017) Thermal structure of the upper atmosphere of Venus simulated by a ground-to-thermosphere GCM. *Icarus* 281:55–72. <https://doi.org/10.1016/j.icarus.2016.09.016>
- Goldstein JJ, Mumma MJ, Kostiuik T, Deming D, Espenak F, Zipoy D (1991) Absolute wind velocities in the lower thermosphere of Venus using infrared heterodyne spectroscopy. *Icarus* 94:45–63. [https://doi.org/10.1016/0019-1035\(91\)90140-0](https://doi.org/10.1016/0019-1035(91)90140-0)
- Gorinov DA, Khatuntsev IV, Zasova LV, Turin AV, Piccioni G (2018) Circulation of Venusian atmosphere at 90–110 km based on apparent motions of the O₂ 1.27 μm nightglow from VIRTIS-M (Venus Express) data. *Geophys Res Lett* 45:2554–2562. <https://doi.org/10.1002/2017GL076380>
- Horinouchi T, Kouyama T, Lee YJ, Murakami S, Ogohara K, Takagi M, Imamura T, Nakajima K, Peralta J, Yamazaki A, Yamada M, Watanabe S (2018) Mean winds at the cloud top of Venus obtained from two-wavelength UV imaging by Akatsuki. *Earth Planets Space* 70(1):10. <https://doi.org/10.1186/s40623-017-0775-3>
- Hoshino N, Fujiwara H, Takagi M, Kasaba Y (2013) Effects of gravity waves on the day–night difference of the general circulation in the Venusian lower thermosphere. *J Geophys Res* 118:1–12. <https://doi.org/10.1002/jgre.20154>
- Imamura T, Ando H, Tellmann S, Pätzold M, Häusler B, Yamazaki A, Sato TM, Noguchi K, Futaana Y, Oschlisniok J, Limaye S, Choudhary RK, Murata Y, Takeuchi H, Hirose C, Ichikawa T, Toda T, Tomiki A, Abe T, Yamamoto Z, Noda H, Iwata T, Murakami S, Satoh T, Fukuhara T, Ogohara K, Sugiyama K, Kashimura H, Ohtsuki S, Takagi S, Yamamoto Y, Hirata N, Hashimoto GL, Yamada M, Suzuki M, Ishii N, Hayashiyama T, Lee YJ, Nakamura M (2017) Initial performance of the radio occultation experiment in the Venus orbiter mission Akatsuki. *Earth Planets Space* 69(1):137. <https://doi.org/10.1186/s40623-017-0722-3>
- Khatuntsev IV, Patsaeva MV, Titov DV, Ignatiev NI, Turin AV, Limaye SS, Markiewicz WJ, Almeida M, Roatsch Th, Moissl R (2013) Cloud level winds from the Venus Express Monitoring Camera imaging. *Icarus* 226:140–158. <https://doi.org/10.1016/j.icarus.2013.05.018>
- Khatuntsev IV, Patsaeva MV, Ignatiev NI, Titov DV, Markiewicz WJ, Limaye SS, Turin AV (2014) Variations of the zonal flow at Venus cloud tops from VMC/VEX UV images in period from 2006 to 2014. In: Abstracts of European Planetary Science Congress 2014. <https://meetingorganizer.copernicus.org/EPSC2014/EPSC2014-177.pdf>
- Khatuntsev IV, Patsaeva MV, Titov DV, Ignatiev NI, Turin AV, Fedorova AA, Markiewicz WJ (2017) Winds in the middle cloud deck from the near-IR imaging by the venus monitoring camera onboard venus express. *J Geophys Res Planets* 122:2312–2327. <https://doi.org/10.1002/2017JE005355>
- Kostiuk T, Livengood TA, Hewagama T, Sonnabend G, Fast KE, Murakawa K, Tokunaga AT, Annen J, Buhl D, Schmuiling F (2005) Titan's stratospheric zonal wind, temperature, and ethane abundance a year prior to Huygens insertion. *Geophys Res Lett* 32:L22205. <https://doi.org/10.1029/2005GL023897>
- Kouyama T, Imamura T, Nakamura M, Satoh T, Futaana Y (2013) Long-term variation in the cloud-tracked zonal velocities at the cloud top of Venus deduced from Venus Express VMC images. *J Geophys Res Planets* 118:37–46. <https://doi.org/10.1029/2011JE004013>
- Krause P, Sornig M, Wischnewski C, Kostiuik T, Livengood TA, Herrmann M, Sonnabend G, Stangier T, Wiegand M, Pätzold M, Mahieux A, Vandaele AC, Piccialli A, Montmessin F (2018) Long term evolution of temperature in the Venus upper atmosphere at the evening and morning terminators. *Icarus* 299:370–385. <https://doi.org/10.1016/j.icarus.2017.07.030>
- Lellouch E, Paubert G, Moreno R, Mouillet A (2008) Monitoring Venus' mesospheric winds in support of Venus Express: IRAM 30-m and APEX observations. *Planet Space Sci* 56:1355–1367. <https://doi.org/10.1016/j.pss.2008.06.010>
- López-Valverde MA, Sonnabend G, Sornig M, Kroet P (2011) Modelling the atmospheric CO₂ 10-μm non-thermal emission in Mars and Venus at high spectral resolution. *Planet Space Sci* 59:999–1009. <https://doi.org/10.1016/j.pss.2010.11.011>
- Mouillet A, Lellouch E, Moreno R, Gurwell M, Sagawa H (2012) Wind mapping in Venus' upper mesosphere with the IRAM-Plateau de Bure interferometer. *Astron Astrophys* 546:A102. <https://doi.org/10.1051/0004-6361/20118451>
- Nakagawa H, Hoshino N, Sornig M, Kasaba Y, Sonnabend G, Stupar D, Aoki S, Murata I (2013) Comparison of general circulation model atmospheric wave simulations with wind observations of Venusian mesosphere. *Icarus* 225:840–849. <https://doi.org/10.1016/j.icarus.2013.02.029>
- Nakagawa H, Aoki S, Sagawa H, Kasaba Y, Murata I, Sonnabend G, Sornig M, Okano S, Kuhn JR, Ritter JM, Kagitani M, Sakano T, Taguchi M, Takami K (2016) IR heterodyne spectrometer MILAHI for continuous monitoring observatory of Martian and Venusian atmospheres at Mt. Haleakala, Hawaii. *Planet Space Sci* 126:34–48. <https://doi.org/10.1016/j.pss.2016.04.002>
- Pätzold M, Häusler B, Bird MK, Tellmann S, Mattei R, Asmar SW, Dehant V, Eidel W, Imamura T, Simpson RA, Tyler GL (2007) The structure of Venus' middle atmosphere and ionosphere. *Nature* 450:657–660. <https://doi.org/10.1038/nature06239>
- Peralta J, Hueso R, Sánchez-Lavega A, Lee YJ, García-Muñoz A, Kouyama T, Sagawa H, Sato TM, Piccioni G, Tellmann S, Imamura T, Satoh T (2017) Stationary waves and slowly moving features in the night upper clouds of Venus. *Nat Astron* 1:0187. <https://doi.org/10.1038/s41550-017-0187>
- Rothman LS, Gordon E, Babikov Y, Barbe A, Chris Benner D, Bernath PF, Birk M, Bizzocchi L, Boudon V, Brown LR, Campargue A, Chance K, Cohen EA, Couderc LH, Devi VM, Drouin BJ, Fayt A, Flaud JM, Gamache RR, Harrison JJ, Hartmann JM, Hill C, Hodges JT, Jacquemart D, Jolly A, Lamouroux J, Le Roy RJ, Li G, Long DA, Lyulin OM, Mackie CJ, Massie ST, Mikhailenko S, Müller HSP, Naumenko OV, Nikitin AV, Orphal J, Perevalov V, Perrin A, Polovtseva ER, Richard C, Smith MAH, Starikova E, Sung K, Tashkun S, Tennyson J, Tyuterev Toon GC, VIG Wagner G (2013) The HITRAN2012 molecular spectroscopic database. *J Quant Spectr Radiat Transf* 130:4–50. <https://doi.org/10.1016/j.jqsrt.2013.07.002>
- Seiff A, Kirk DB (1982) Structure of the Venus mesosphere and lower thermosphere from measurements during entry of the pioneer Venus probes. *Icarus* 49:49–70. [https://doi.org/10.1016/0019-1035\(82\)90056-2](https://doi.org/10.1016/0019-1035(82)90056-2)

- Seiff A, Kirk DB, Young RE, Blanchard RC, Findlay JT, Kelly GM, Sommer SC (1980) Measurements of thermal structure and thermal contrasts in the atmosphere of Venus and related dynamical observations—results from the four Pioneer Venus probes. *J Geophys Res* 85:7903–7933. <https://doi.org/10.1029/JA085iA13p07903>
- Seiff A, Schofield JT, Kliore AJ, Taylor FW, Limaye SS, Revercomb HE, Sromovsky LA, Kerzhanovich VV, Moroz VI, Ya Marov M (1985) Models of the structure of the atmosphere of Venus from the surface to 100 kilometers altitude. *Adv Space Res* 5:3–58. [https://doi.org/10.1016/0273-1177\(85\)90197-8](https://doi.org/10.1016/0273-1177(85)90197-8)
- Sonnabend G, Sornig M, Schieder R, Kostiuik T, Delgado J (2008) Temperatures in Venus upper atmosphere from mid-infrared heterodyne spectroscopy of CO₂ around 10 μm wavelength. *Planet Space Sci* 56:1407–1413. <https://doi.org/10.1016/j.pss.2008.05.008>
- Sonnabend G, Kroetz P, Sornig M, Stupar D (2010) Direct observations of Venus upper mesospheric temperatures from ground based spectroscopy of CO₂. *Geophys Res Lett* 37:L11102. <https://doi.org/10.1029/2010GL043335>
- Sonnabend G, Krötz P, Schmülling F, Kostiuik T, Goldstein J, Sornig M, Stupar D, Livengood T, Hewagama T, Fast K, Mahieux A (2012) Thermospheric/mesospheric temperatures on Venus: results from ground-based high-resolution spectroscopy of CO₂ in 1990/1991 and comparison to results from 2009 and between other techniques. *Icarus* 217:856–862. <https://doi.org/10.1016/j.icarus.2011.07.015>
- Sornig M, Livengood T, Sonnabend G, Kroetz P, Stupar D, Kostiuik T, Schieder R (2008) Venus upper atmosphere winds from ground-based heterodyne spectroscopy of CO₂ at 10 μm wavelength. *Planet Space Sci* 56:1399–1406. <https://doi.org/10.1016/j.pss.2008.05.006>
- Sornig M, Livengood TA, Sonnabend G, Stupar D, Kroetz P (2012) Direct wind measurements from November 2007 in Venus' upper atmosphere using ground-based heterodyne spectroscopy of CO₂ at 10 μm wavelength. *Icarus* 217:863–874. <https://doi.org/10.1016/j.icarus.2011.03.019>
- Sornig M, Sonnabend G, Stupar D, Kroetz P, Nakagawa H, Mueller-Wodarg I (2013) Venus' upper atmospheric dynamical structure from ground-based observations shortly before and after Venus' inferior conjunction 2009. *Icarus* 225:828–839. <https://doi.org/10.1016/j.icarus.2012.12.005>
- Stangier T (2015) Atmospheric thermal properties of Venus and Mars. Investigation of CO₂ absorption lines using ground-based mid-infrared heterodyne spectroscopy. Ph.D. thesis, Univ. Köln. <https://kups.uni-koeln.de/5972/>
- Stangier T, Hewagama T, Sornig M, Sonnabend G, Kostiuik T, Herrmann M, Livengood T (2015) Thermal structure of Venus' nightside mesosphere as observed by infrared heterodyne spectroscopy at 10 μm. *Planet Space Sci* 113:359–368. <https://doi.org/10.1016/j.pss.2015.01.021>

Publisher's Note

Springer Nature remains neutral with regard to jurisdictional claims in published maps and institutional affiliations.

Submit your manuscript to a SpringerOpen[®] journal and benefit from:

- Convenient online submission
- Rigorous peer review
- Open access: articles freely available online
- High visibility within the field
- Retaining the copyright to your article

Submit your next manuscript at ► [springeropen.com](https://www.springeropen.com)
